5-10-1998

Theory of Quasi-Equilibrium Nucelosynthesis and Applications to Matter Expanding from High Temperature and Density

Bradley S. Meyer
Clemson University

Tracy D. Krishnan
Clemson University

Donald D. Clayton
Clemson University, claydonald@gmail.com

THE ASTROPHYSICAL JOURNAL, 498:808–830, 1998 May 10

THEORY OF QUASI-EQUILIBRIUM NUCLEOSYNTHESIS AND APPLICATIONS TO MATTER EXPANDING FROM HIGH TEMPERATURE AND DENSITY

BRADLEY S. MEYER, TRACY D. KRISHNAN, AND DONALD D. CLAYTON
Department of Physics and Astronomy, Clemson University, Clemson, SC 29634-1911
Received 1997 March 14; accepted 1997 December 19

ABSTRACT

Our first purpose is construction of a formal theory of quasi-equilibrium. We define quasi-equilibrium, in its simplest form, as statistical equilibrium in the face of an extra constraint on the nuclear populations. We show that the extra constraint introduces a uniform translation of the chemical potentials for the heavy nuclei and derive the abundances in terms of it. We then generalize this theory to accommodate any number of constraints. For nucleosynthesis, the most important constraint occurs when the total number of heavy nuclei Y_h within a system of nuclei differs from the number that would exist in nuclear statistical equilibrium (NSE) under the same conditions of density and temperature. Three situations of high relevance are (1) silicon burning, wherein the total number of nuclei exceeds but asymptotically approaches the NSE number; (2) alpha-rich freezeout expansions of high entropy, wherein Y_h is less than the NSE number; and (3) expansions from high temperature of low-entropy matter, in which Y_h exceeds the NSE number. These are of importance, respectively, within (1) supernova shells, (2) Type II supernova cores modestly outside the mass cut, and (3) Type Ia supernova cores in near–Chandrasekhar-mass events.

Our next goal is the detailed analysis of situation (2), the high-entropy alpha-rich neutron-rich freezeout. We employ a nuclear reaction network, which we integrate, to compare the actual abundances with those obtained at the same thermal conditions by the quasi-equilibrium (QSE) theory and by the NSE theory. For this detailed comparison, we choose a high-entropy photon-to-nucleon ratio $\phi = 6.8$, for which we conduct expansions at initial bulk neutron excess $\eta_0 = 0.10$. We demonstrate that the abundance populations, as they begin expansion and cooling from temperature 10×10^9 K, are characterized by three distinct phases: (1) NSE, (2) QSE having Y_h smaller than the NSE value, and (3) final reaction rate–dependent freezeout modifications of the QSE. We demonstrate that the true final abundances are well approximated by the QSE distribution near the freezeout temperature $T_{9f} = 4.0$. During the expansion, the QSE distribution changes shape continuously in ways that are independent of the reaction cross sections of the heavy nuclei with free light particles. It is this changing shape, rather than "nuclear flows," that establish the abundance pattern. The abundance pattern is actually determined by the parameter Y_h and the degree to which it differs from the NSE value owing to the slowness with which light particles can be assembled into heavy nuclei ($A \geq 12$). We also detail the nature and magnitude of the freezeout corrections to the QSE distribution. The entire distribution depends less upon the values of heavy-element cross sections than has been heretofore thought.

Our third goal is to survey the alpha-rich freezeout. We do this by less complete analysis of nine different expansions determined by the matrix of three distinct entropies ($\phi = 1.7$, 6.8, and 17) and three distinct initial neutron excesses ($\eta_0 = 0.003$, 0.10, and 0.1667). The trends are easily comprehended in terms of the concept of quasi-equilibrium, whereas they are not understandable in terms of either NSE or in terms of reaction rates. This secures for the QSE concept a major diagnostic capability within nucleosynthesis theory. We delineate the key trends and also remark on the ways that order arises from disorder in this complex system. We conclude with a discussion of how such systems assemble heavy nuclei.

Subject headings: nuclear reactions, nucleosynthesis, abundances — supernovae: general

1. INTRODUCTION

The notion of statistical equilibrium of nuclear species has played an immense intellectual role in the theory of nucleosynthesis. Hoyle (1946) launched the paradigm of stellar nucleosynthesis by arguing that the thermal conditions in highly evolved massive stars would be suitable for the establishment of nuclear statistical equilibrium (NSE). He went on to show that ^{56}Fe could be the most abundant nucleus if the neutron-to-proton ratio took on the correct value, near $Z/N = 0.87$. This was named the *e*-process by Burbidge et al. (1957). Its appropriateness was defended for a decade by those authors until new concepts indicated that nature preferred a much smaller neutron excess (nearly zero) and synthesized most ^{56}Fe as its radioactive ^{56}Ni parent. The history of this has been described (Clayton 1998), and the astrophysical status was reviewed by Meyer in Wallerstein et al. (1997). If the entropy of the expanding matter is not too large, the equilibrium adjusts in small ways as the temperature drops, narrowing the abundance peak and altering odd/even abundance ratios. Near $T = 4 \times 10^9$ K, the nuclear reactions become too slow to maintain equilibrium at lower temperature; but the effect is not very important. The equilibrium at the freezeout temperature (near $T_9 = 4$) cannot be much altered by the few reactions that still occur with free protons and neutrons and alpha particles because they are of such small abundance in comparison with the abundances of the dominant heavy nuclei. The final abundances resemble closely the equi-

librium abundances at the freezeout temperature. Almost all of the matter was contained in the equilibrium abundance peak.

The nuclear evolution of the star presented a natural obstacle to the attainment of NSE via the sequential burning phases that occur. That obstacle was ^{28}Si and its conversion into ^{56}Ni. Bodansky, Clayton, & Fowler (1968) were able to show that the close approach of all reaction rates involving n, p, and α to the rates of their inverse reactions established a type of restricted nuclear equilibrium, which they termed "nuclear quasi-equilibrium" (QSE). The entire abundance distribution between ^{28}Si and ^{56}Ni (and a few others) took on a quasi-static character in which its shape did not change over times sufficient to allow huge numbers of individual reactions to occur. Its shape was frozen by the balance of reactions with their inverse reactions. It could evolve only as the refractory ^{28}Si slowly melted away, replaced by a ^{56}Ni abundance peak. This is well known, and our point here is that this quasi-static evolution is governed by a single parameter, which they took to be the ratio $Y(^{28}\mathrm{Si})/Y(^{56}\mathrm{Ni})$. Its value was seen as a parameter that fixed the entire abundance distribution (see also Clayton 1983). That ratio taken as the governing parameter began with a huge value (almost pure ^{28}Si) and finished with an infinitesimal value (almost pure ^{56}Ni). That silicon-burning evolution could equally have utilized as its parameter Y_h, the number of heavy nuclei, which decreases by a factor of 2 during the burning. But the rates of individual (α, n), (α, p), (p, n), (p, γ), (n, γ), and (α, γ) and their inverses played almost no role for nuclei between ^{28}Si and ^{56}Ni. In this insensitivity to nuclear reactions, this burning process showed the same indifference that was first found in NSE long before. The reactions were found to determine a more subtle distinction, namely, how the QSE decomposes into two or more smaller QSE clusters (Woosley, Arnett, & Clayton 1973; Hix & Thielemann 1996).

When higher entropy expansions were studied, the situation changed in a profound way. At such relatively low density and high temperature, the matter is decomposed to an equilibrium broth of nucleons and alpha particles; but owing also to the low density, those particles cannot collide often enough to recombine into heavy nuclei in the time available during the expansion. It was found in those cases that the mass of heavy nuclei did not completely dominate, but there exist free alpha particles at the end of the expansion. This was called the "alpha-rich freezeout" (e.g., Woosley et al. 1973). What makes it so important is that in the O and Si shells of evolved massive stars, the outgoing shock wave after core bounce is so strong that those shells are heated to such a high temperature that their high entropy places them in the regime of the alpha-rich freezeout. The ^{56}Ni nucleosynthesis within Type II supernovae appears to be of this type (e.g., Thielemann, Hashimoto, & Nomoto 1990).

In this paper we study alpha-rich freezeouts at high entropy and at substantial neutron richness. This was first done by Woosley & Hoffman (1992), who called it "the alpha process." In so doing they hoped to simultaneously call attention to the alpha-rich nature of the freezeout and to the neutron richness of the bath, which greatly expands the range of abundant nuclei produced. Woosley & Hoffman apparently thought that (α, n)-reactions on neutron-rich isotopes played a large role in the abundances produced. One of our results will show that a language appealing to alpha reactions carrying the nuclear flow to larger and more neutron-rich nuclei is inappropriate. We will demonstrate that the matter is organized by a QSE distribution in which individual reaction rates are of little importance and in which alpha reactions play no special role. We follow the lead of Meyer, Krishnan, & Clayton (1996) in this, for they showed the QSE nature of the resulting abundance distributions in their study of the origin of ^{48}Ca.

Over and beyond these and other demonstrations, moreover, we present a theory of QSE as a statistical equilibrium with one extra constraint. This theory is cast into a form closely resembling the theory of thermodynamic equilibrium. This theory will allow explicit understanding of the controlling importance of the abundance parameter Y_h, defined as the abundance sum of heavy nuclei ($A \geq 12$) per nucleon of matter. It clarifies the simple way in which the free energy decreases, or equivalently, the entropy increases as Y_h increases. This may be viewed as a natural struggle to attain thermodynamic equilibrium against steep odds.

Broad intellectual relevance may exist in the relationship of this study to a modern scientific thrust called "the search for the laws of self-organization and complexity" (Kauffman 1995). Kauffman, one of the pioneers of this movement and a member of the Santa Fe Institute for the study of complexity, finds the origins of life in the attractive hypothesis that natural selection achieves genetic regulatory networks that lie near the edge of chaos. He envisions a phase transition between order and chaos and that life exists at the edge of chaos. Though differing from chaos, the transition from equilibrium to disequilibrium carries many similar features. The words of Kauffman are rewardingly read with our present study, rather than the origin of life, in mind: "The best exploration of an evolutionary space occurs at a kind of phase transition between order and disorder, when populations begin to melt off the local peaks they have become fixated on and flow along ridges toward distant regions of higher fitness" (p. 27). We will return to this in our analysis of Figure 10 in § 3.3.

Our calculations begin with matter in equilibrium, consisting of mostly neutrons and protons and the populations of heavy nuclei in statistical equilibrium with those free particles. Population migration is driven by the unidirectional temporal arrow–expansion and cooling. A first systemic transition occurs when the number of heavy nuclei cannot keep pace with the entropy maximum demanded by randomness. After that transition, the populations exist in a quasi-equilibrium with the free particles and the (momentarily) fixed number Y_h of heavy nuclei. A second transition occurs later as individual reaction rates become sufficiently slow that they are unable to remain equal to their inverse reactions. At that time the quasi-equilibrium also breaks down. The single, large quasi-equilibrium cluster decomposes into several smaller clusters. This is followed by a series of unidirectional shifts in populations that are usually called freezeout in astrophysics because they are terminated by ineffective slowness of all reactions below a freezeout temperature. At this final moment, the populations stand far removed from the expectations of equilibrium. They have a certain order in that "the fittest" have dominated. The "order" is in some cases as bizarre as the dominance of Kr or Sr nuclei at the end of evolution, whereas the disorder is the familiar state of thermodynamic equilibrium (maximum disorder). The fitness of the winners

is decided in a lengthy evolutionary battle with the other heavy species. Their own populations depend upon the fitness not only of all other abundant species but also upon the fitness of previously abundant ancestors, now extinct or unimportant.

2. THEORETICAL FRAMEWORK

In this section we develop the theoretical structure underlying quasi-equilibrium nucleosynthesis. We apply our results to actual network calculations in § 3.

2.1. *General Considerations*

Because we will specify the temperature T in our network calculations, we will consider a system in contact with a heat bath. For such a system, infinitesimal changes in the Helmholtz free energy f per nucleon are given by

$$df = -sdT - Pdv + \sum_i \mu_i dY_i , \tag{1}$$

where s is the entropy per nucleon, P is the pressure, v is the volume per nucleon, μ_i is the chemical potential of species i, Y_i is the abundance of species i per nucleon, and the sum runs over all species present. We seek the equilibrium at constant temperature and volume; thus, equation (1) becomes

$$df = \sum_i \mu_i dY_i . \tag{2}$$

In most nucleosynthetic environments, the species present are nucleons and nuclei, electrons and positrons, neutrinos, and photons. The chemical potential of photons is zero as is that of the neutrinos, since they are generally decoupled from the matter and are free streaming. Under these circumstances, equation (2) becomes

$$df = \sum_i^{\text{nuclear}} \mu_i dY_i + \mu_e dY_e , \tag{3}$$

where the sum runs only over nuclear species and where Y_e is the abundance of net electrons (that is, electrons in excess of positrons) per nucleon. In what follows, we will assume for simplicity that the electron fraction Y_e is fixed ($dY_e = 0$) since it changes very slowly on the timescale of other nuclear reactions that are occurring, and we will drop the "nuclear" on the sum in equation (3).

The tendency of an system in contact with a heat bath at temperature T is to evolve to a condition of minimum free energy. For the nucleosynthetic system, this is nuclear statistical equilibrium. In this case, the free energy is stationary under any infinitesimal rearrangement of the abundances Y_i:

$$\sum_i \mu_i^{\text{NSE}} dY_i = 0 , \tag{4}$$

where μ_i^{NSE} is the chemical potential of the species i in NSE. Subtracting equation (4) from equation (3) with $dY_e = 0$ yields

$$df = \sum_i (\mu_i - \mu_i^{\text{NSE}}) dY_i . \tag{5}$$

Because the nuclear species are nonrelativistic and nondegenerate under nearly all conditions relevant for nucleosynthesis, the appropriate chemical potential is that for an ideal Boltzmann gas:

$$\mu_i = m_i c^2 + kT \ln\left[\frac{\rho N_A Y_i}{G_i}\left(\frac{2\pi\hbar^2}{m_i kT}\right)^{3/2}\right], \tag{6}$$

where m_i and G_i are the mass and partition function of species i, respectively, c is the speed of light, k is Boltzmann's constant, ρ is the mass density, N_A is Avogadro's number, and $2\pi\hbar$ is Planck's constant. Since we compare abundances at the same temperature and density, equation (5) becomes

$$df = kT \sum_i \ln(Y_i/Y_i^{\text{NSE}}) dY_i . \tag{7}$$

This equation elegantly summarizes the second law for nucleosynthetic systems. It clearly shows that the system will tend to evolve toward the state in which all abundances are given by their NSE values. The change dY_i contributes to the requirement $df \leq 0$ by increasing Y_i if $Y_i < Y_i^{\text{NSE}}$ and by decreasing Y_i if $Y_i > Y_i^{\text{NSE}}$.

2.2. *Quasi-Equilibrium*

The minimum free energy state of a nucleosynthetic system is subject to certain constraints. First, the total number of nucleons in the system is fixed. This is equivalent to the requirement that the sum of the mass fractions of all nuclear species must be unity:

$$\sum_i A_i Y_i = 1 , \tag{8}$$

where A_i is the mass number of species i. Also, since we have taken Y_e to be fixed, charge neutrality requires

$$\sum_i Z_i Y_i = Y_e , \tag{9}$$

where Z_i is the proton number of species i. It is convenient to subtract equation (9) from equation (8) to obtain the separate, but not independent, constraint that

$$\sum_i N_i Y_i = 1 - Y_e . \tag{10}$$

This constraint is simply the requirement that the total number of neutrons per nucleon is fixed, just as equation (9) is the constraint that the total number of protons per nucleon is fixed.

As suggested by the results in Meyer et al. (1996), QSE (as we here define it) is a minimum free energy state when the number of nuclei differs from that demanded by NSE. We must thus add a third constraint, namely, that the total number of heavy nuclei Y_h is fixed. By heavy nuclei, we mean nuclei with $A \geq 12$. In practice, because the abundances of all nuclear species other than neutrons (n), protons (p), and alpha particles (α) with $A < 12$ are typically negligibly small, we write this constraint as

$$\sum_{i \neq n,\, p,\, \alpha} Y_i = Y_h . \tag{11}$$

We seek the abundances that minimize the free energy subject to the three constraints.

Our goal is most easily achieved through the method of Lagrange multipliers. We first define three functions that embody the three constraints:

$$g_p = Y_e - \sum_i Z_i Y_i , \tag{12}$$

$$g_n = 1 - Y_e - \sum_i N_i Y_i , \tag{13}$$

and

$$g_h = Y_h - \sum_{i \neq n,\, p,\, \alpha} Y_i \,. \tag{14}$$

We accommodate these constraints with three Lagrange multipliers: λ_p, λ_n, and λ_h. The problem of finding the abundances that minimize the free energy thus becomes that of finding the abundances for which the function $f + \lambda_p g_p + \lambda_n g_n + \lambda_h g_h$ is stationary and $g_p = g_n = g_h = 0$. For this purpose, Y_e and Y_h are not variables, but constants characterizing the solution. From equations (3), (12), (13), and (14), we find

$$\sum_{i=n,\, p,\, \alpha} (\mu_i - Z_i \lambda_p - N_i \lambda_n) dY_i + \sum_{i \neq n,\, p,\, \alpha} (\mu_i - Z_i \lambda_p - N_i \lambda_n - \lambda_h) dY_i = 0 \,. \tag{15}$$

Because we have introduced three new as yet undetermined parameters (the Lagrange multipliers), we may now vary the abundances independently; thus, each term in the sum must separately be zero. For the neutrons, $Z = 0$ and $N = 1$, so clearly $\lambda_n = \mu_n$. Similarly, for protons, $Z = 1$ and $N = 0$, so $\lambda_p = \mu_p$. These results thus require for the heavy nuclei that

$$\mu_i = \lambda_h + Z_i \mu_p + N_i \mu_n \,. \tag{16}$$

For the corresponding solution of NSE, the number of heavy nuclei is not constrained so that $\lambda_h = 0$; thus

$$\mu_i^{\rm NSE} = Z_i \mu_p^{\rm NSE} + N_i \mu_n^{\rm NSE} \,. \tag{17}$$

This is the well-known condition for NSE (see, e.g., Arnett 1996) and allows for solution of the NSE abundances. Subtracting this equation from equation (16) then yields

$$\mu_i - \mu_i^{\rm NSE} = \lambda_h + Z_i(\mu_p - \mu_p^{\rm NSE}) + N_i(\lambda_n - \lambda_n^{\rm NSE}) \,. \tag{18}$$

With the definition of the chemical potential in equation (6), equation (18) becomes

$$\ln(Y_i/Y_i^{\rm NSE}) = \lambda_h/kT + Z_i \ln(Y_p/Y_p^{\rm NSE}) + N_i \ln(Y_n/Y_n^{\rm NSE}) \,. \tag{19}$$

Solving for Y_i thus yields

$$Y_i = e^{\lambda_h/kT} R_p^{Z_i} R_n^{N_i} Y_i^{\rm NSE} \,, \tag{20}$$

where $R_p = Y_p/Y_p^{\rm NSE}$ and $R_n = Y_n/Y_n^{\rm NSE}$ measure the overabundance of free nucleons with respect to their NSE abundances (presumed already known from T, ρ, and Y_e). Solution of the QSE abundances in equation (20) then requires finding the three quantities λ_h, R_p, and R_n such that the three constraints are satisfied, that is, that $g_p = g_n = g_h = 0$.

Equation (20) usefully expresses the abundances of the various species in QSE in terms of the NSE abundances. The Lagrange multiplier λ_h clearly plays an important role in the QSE abundances. It has a natural interpretation, which we present in the next subsection. For now, we note that the ratio of abundances of two heavy nuclei in QSE can be expressed in terms of their NSE ratio (Woosley, Arnett, & Clayton 1973; Meyer et al. 1996)

$$\frac{Y_j}{Y_i} = R_p^{Z_j - Z_i} R_n^{N_j - N_i} \left(\frac{Y_j^{\rm NSE}}{Y_i^{\rm NSE}} \right) . \tag{21}$$

For completeness, we note that the abundance of alpha particles within the QSE solution may also be found from equation (15). The result for exact QSE is simply

$$R_\alpha = R_p^2 R_n^2 \,, \tag{22}$$

where $R_\alpha = Y_\alpha/Y_\alpha^{\rm NSE}$ (see also Meyer et al. 1996).

2.3. *Interpretation of* λ_h

In order to interpret λ_h, we substitute equation (19) into equation (7). This yields

$$df = \lambda_h dY_h + kT \sum_i \ln(R_p^{Z_i} R_n^{N_i}) dY_i \,. \tag{23}$$

For strict QSE, the sum in equation (23) will be zero for any rearrangement of abundances among n's, p's, or α's or among the heavy nuclei. For example, the rearrangement $2p + 2n \rightarrow \alpha$ would give $dY_n = dY_p$ and $dY_p = -2dY_\alpha$; hence, using $Z_p = 1$, $N_p = 0$, $Z_n = 0$, $N_n = 1$, and $Z_\alpha = N_\alpha = 2$, the sum is

$$\ln R_p \, dY_p + \ln R_n \, dY_n + \ln(R_p^2 R_n^2) dY_\alpha = (-2 \ln R_p - 2 \ln R_n + 2 \ln R_p + 2 \ln R_n) dY_\alpha = 0 \,. \tag{24}$$

In similar fashion, a rearrangement among the heavy nuclei would be $i + (Z_j - Z_i)p + (N_j - N_i)n \rightarrow j$. In this case, $dY_j = -dY_i$, $dY_p = -(Z_j - Z_i)dY_j$, and $dY_n = -(N_j - N_i)dY_j$, and the sum again yields zero. In strict QSE, we therefore conclude

$$df = \lambda_h dY_h \,. \tag{25}$$

By recalling equation (2), we naturally associate the Lagrange multiplier λ_h with the chemical potential of heavy nuclei taken as a whole:

$$\lambda_h = \mu_h \,. \tag{26}$$

With this, the QSE abundances thus become

$$Y_i = e^{\mu_h/kT} R_p^{Z_i} R_n^{N_i} Y_i^{\rm NSE} \,. \tag{27}$$

Meyer et al. (1996) pointed out that the dynamics of QSE are governed by how the number of heavy nuclei evolves. The number of heavy nuclei tends to evolve toward the number that the system would have in NSE. The chemical potential μ_h provides a more precise diagnostic for the dynamics of the QSE because μ_h represents the free energy "cost" of adding a heavy nucleus. If μ_h is zero, there is no net free energy loss or gain in adding a heavy nucleus. This is NSE. If $\mu_h < 0$, it is energetically advantageous for the system to add nuclei. As equation (25) shows in this case, the system will increase the number of heavy nuclei in order to decrease the free energy. The system will tend to destroy heavy nuclei, however, if $\mu_h > 0$. Here it "costs too much" to have so many nuclei. It is essential in these considerations to note that the equilibrium among the heavy nuclei means that they are all linked together into a single abundance entity. For this reason, a single quantity, viz., μ_h, conveniently (and fundamentally) characterizes its energetics.

The chemical potential μ_h is not so convenient a parameter when the heavy nuclei are not in QSE. We obtain μ_h as part of the global solution of the QSE (or NSE). When the heavy nuclei are not in QSE, μ_h is a much more difficult quantity to obtain or even define. This is not surprising, since in this case it makes little sense to think of the heavy nuclei as all linked together. Nevertheless, as we shall see, QSE is an excellent description of the abundances throughout much of the expansion of matter from high temperature,

and μ_h provides a valuable probe of the dynamics of the QSE. On the other hand, the QSE approximation fails in certain regards, and this failure provides us with important insights. Even here, however, μ_h is an important diagnostic for understanding how the system is evolving.

2.4. *General Theory*

In the previous subsections, we have developed the theory of the most basic QSE, namely, the one with a constraint on the total number of heavy nuclei. It is, however, quite straightforward to generalize the theory. For example, in silicon burning two distinct QSE clusters develop—one containing Si and one containing Ni (Woosley, Arnett, & Clayton 1973; Hix & Thielemann 1996). In this equilibrium, the number of nuclei Y_{h1} in cluster 1 and the number of nuclei Y_{h2} in cluster 2 are both constrained. This, however, effectively adds only one constraint because Y_{h1} and Y_{h2} are related by $Y_h = Y_{h1} + Y_{h2}$. For this equilibrium, the constraints would be those from equation (9), equation (10), and two constraints arising from the fixed number of nuclei in each of the two clusters:

$$Y_{h1} = \sum_{i \in \text{cluster 1}} Y_i \tag{28}$$

and

$$Y_{h2} = \sum_{i \in \text{cluster 2}} Y_i \,. \tag{29}$$

The two constraints in equations (28) and (29) have replaced the single constraint in equation (11). The free energy minimization now requires four Lagrange multipliers: λ_f, λ_g, λ_{h1}, and λ_{h2}. By operations similar to those in § 2.2, and by interpretation of λ_{h1} and λ_{h2} as in § 2.3, we now find

$$Y_i^{(1)} = e^{\mu_1/kT} R_p^{Z_i} R_n^{N_i} Y_i^{\rm NSE} \tag{30}$$

and

$$Y_i^{(2)} = e^{\mu_2/kT} R_p^{Z_i} R_n^{N_i} Y_i^{\rm NSE} \,, \tag{31}$$

where the superscript (1) in equation (30) refers to cluster 1 and the superscript (2) in equation (31) refers to cluster 2. The chemical potentials μ_1 and μ_2 play an exactly analogous role to μ_h but for clusters 1 and 2, respectively.

The procedure outlined above may be extended to accommodate three, four, or any number of equilibrium clusters. Each additional cluster adds a constraint on the free energy minimum and introduces a new chemical potential to account for the energetics of the new cluster. Thus, the theory presented here is completely general. It can accommodate, for example, (n, γ)-(γ, n) equilibrium in the *r*-process, where each cluster is simply the set of isotopes of a given element in equilibrium under exchange of neutrons.

With this theoretical framework for QSE laid out, we now turn to some applications to network calculations. In what follows, we focus strictly on the basic QSE, that is, the one developed in §§ 2.2–2.3, because it is the most essential one for understanding the nuclear dynamics of matter expanding from high temperature. We return to the question of multiple equilibrium clusters in the Conclusion (§ 6), where we discuss the emergence of order in nucleosynthetic systems.

3. NETWORK CALCULATIONS

In this section we present network calculations of the nucleosynthesis occurring in matter expanding from high temperature and density and an analysis of them in light of our understanding of QSE.

3.1. *Details of the Calculations*

The nuclear network code is that described in Meyer et al. (1996). We have made some improvements in it, however. Most importantly, we now compute all reverse reaction rates from detailed balance in a more consistent manner. For example, Caughlan & Fowler (1988) give reverse reaction ratios. Instead of using these reverse ratios, we now compute them from our set of nuclear masses and nuclear partition functions. In some cases, the reverse ratios we compute differ slightly from those presented in Caughlan & Fowler (1988). Although the differences are typically small, we gain internal consistency. Now the abundances governed by the nuclear rates (without weak interactions) evolve into a steady state NSE that is precisely the same equilibrium that we compute with our NSE subroutine. This allows for much better comparison between the network results and NSE and for more accurate computation of QSE.

In the course of making these changes, we discovered errors in matrix element assignments for two reactions. These two matrix elements each contained one too many powers of the density. While these reactions were minor, they did have an effect on the timescale for establishment of NSE. The consequence is that the pre-NSE phase, the phase needed for establishment of NSE, is of much shorter duration than indicated by the results in Meyer et al. (1996). The main conclusions of Meyer et al. (1996) regarding ^{48}Ca synthesis are in no way altered by these errors, but the lesson is that there are potential perils in comparing the results of network evolutions with NSE. Nevertheless, there are great advantages in such an exercise, for it is only by carefully comparing the code to the NSE results that we were able to uncover these errors in matrix element assignments. We now compute all matrix elements automatically, which eliminates the possibility of such errors.

The actual network is the same as in Meyer et al. (1996) (see Table 1 of that paper for the nuclei included). This network includes nearly all isotopes from the proton-drip to neutron-drip lines for elements ranging from hydrogen to tin. All calculations that we present here were parameterized in terms of constant photon-to-nucleon ratio ϕ. This quantity is

$$\phi = 0.34 \, \frac{T_9^3}{\rho_5} \,, \tag{32}$$

where $T_9 = T/10^9$ K and $\rho_5 = \rho(\text{g cm}^{-3})/10^5$. Since all of our calculations are constrained to constant ϕ, it is clear that throughout each expansion the density behaved as $\rho \propto T^3$. It is useful to note that ϕ is directly proportional to the entropy per nucleon in photons. For this reason, ϕ increases monotonically with increasing s.

The other parameters in our expansions were the neutron excess and the expansion timescale. Each calculation began at $T_9 = 10$ with a chosen initial neutron excess η_0. We began with a mixture of alpha particles and neutrons, but the matter quickly attains NSE so that our results, for given η_0, do not depend on the specific choice of initial abundances. During the course of each expansion, the neutron richness changed due to electron capture and β^+ and β^- decay. We took the mass density to fall exponentially with

the time during the expansion with an e-folding time given by 0.2 s. The calculations ran until the neutron abundance per nucleon fell below 10^{-30}. By this point, the nuclear reactions had frozen out.

We analyze a set of nine calculations. We chose to study expansions with $\phi = 1.7$, 6.8, and 17. These choices enable comparison with the calculations of Woosley & Hoffman (1992). For each ϕ, we chose initial $\eta_0 = 0.03$, 0.10, and 0.1667. To clarify the behavior of each expansion, we discuss in detail the expansion $\phi = 6.8$ and $\eta_0 = 0.10$. First, however, we explore the timescale necessary to achieve NSE.

3.2. *Timescale to Achieve NSE*

We begin our analysis of our network calculations by finding the timescale needed to achieve NSE. Figure 1 shows R_n and R_α as functions of time at the very early stages of the expansion with $\phi = 6.8$ and $\eta_0 = 0.10$. Both of these quantities, though initially far from unity (their NSE values), converge on unity within ~ 1 μs. NSE is quickly achieved. This conclusion is in contrast with the erroneous finding of a longer pre-NSE phase in Meyer et al. (1996), as shown in their Figure 8. As mentioned above, the matrix elements for two reactions on low-abundance species each had an extra power of density, which made the timescale for the network to achieve NSE incorrectly long.

The timescale of ~ 1 μs to achieve NSE is also clear from Figure 2, which shows μ_h/kT as a function of time in the early stages of the expansion. Within about 1 μs, μ_h/kT locks into a value of zero. This is the value in NSE. The other expansions have similarly short timescales to get into NSE. The practical consequence is that the matter quickly attains NSE in all of our expansions, so that our results do not depend on the specific choice of initial abundances.

3.3. *Details of the Reference Expansion*

The reference calculation had $\phi = 6.8$ and $\eta_0 = 0.10$. For each 10 time steps in this expansion, we computed NSE from T_9, ρ, and the instantaneous value of Y_e in the network. From the NSE abundances and the instantaneous value of Y_h, we then computed the QSE abundances (see eq. [27]). This allows fruitful comparison of the network abundances with NSE and QSE. It also provides a number of useful diagnostics to help clarify the nuclear dynamics of this expansion.

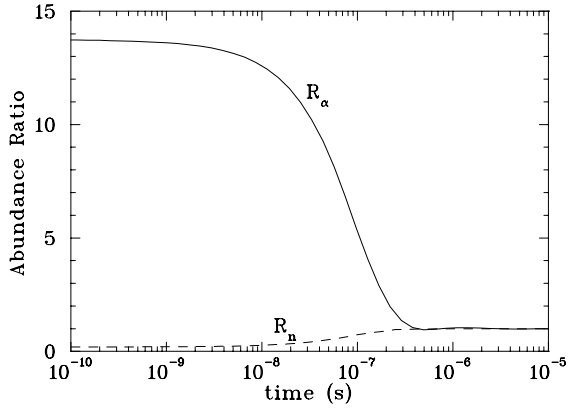

FIG. 1.—Prompt relaxation of free nucleons and alpha particles to their NSE values at $T_9 = 10$. This initial composition was taken as alpha particles plus enough neutrons to provide the neutron excess. R_α and R_n measure the ratio of the true number densities to those obtained in NSE at $T_9 = 10$ and $\rho = 5 \times 10^6$ g cm^{-3}. Evidently the network solution relaxes to the NSE values ($R = 1$) within a microsecond. The free-proton ratio R_p closely resembles R_n.

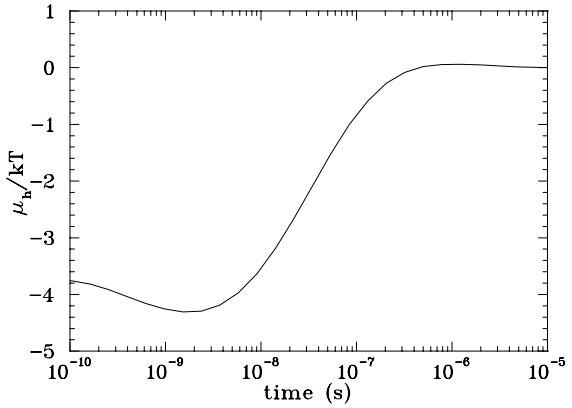

FIG. 2.—Prompt relaxation of the chemical potential of heavy nuclei to its NSE value at initial $T_9 = 10$ and $\rho = 5 \times 10^6$ g cm^{-3}. Because the initial abundances contained no heavy nuclei Y_h, it is energetically advantageous to create some, so that μ_h is initially negative. Within a microsecond, however, μ_h also has relaxed to zero, its value in NSE. Figs. 1 and 2 taken together show that NSE is established within 10^{-6} s, which is 5 orders of magnitude faster than the expansion timescale. Interestingly, but unimportantly, in the initial rush to create heavy nuclei the network first makes a few too many C nuclei before the reverse flow from heavier nuclei settles in, so that μ_h overshoots zero slightly and then relaxes back down to equilibrium.

The first diagnostic is X_α, the mass fraction of alpha particles, during the expansion. This is shown in Figure 3, which gives X_α for the network expansion, NSE, and QSE. In this and subsequent figures, the network solution (the correct solution) is always the solid curve, the NSE solution

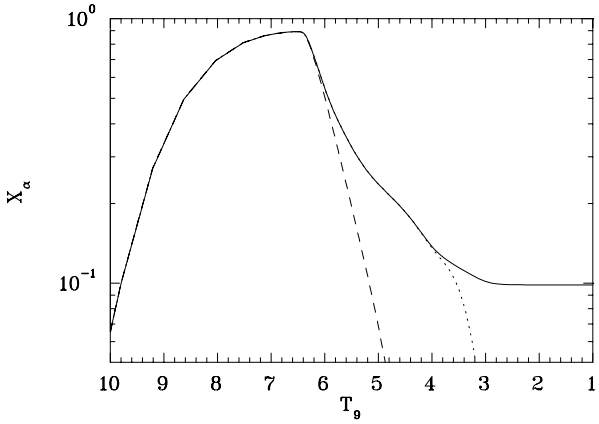

FIG. 3.—Mass fraction of free alpha particles as the matter expands and cools. In broad outline, the alpha-particle density first rises as the temperature declines and later falls again to a final asymptotic value. Time is related to temperature by $t = 0.6s \ln(10/T_9)$. Thermal conditions are constrained to maintain constant photon-to-nucleon ratio ϕ. The "true solution," as given by the complete nuclear network, is shown as a solid curve. The alpha fraction in NSE at that T is the long-dashed curve, while the QSE alpha fraction at T is shown as the dotted curve. All three solutions are in exact agreement after the first microsecond down to $T_9 = 6.4$ ($t = 0.226$ s). As T_9 falls below 6.4, the alpha density begins to exceed NSE expectations by increasingly large factors, marking the breakdown of NSE. The QSE solution, however, continues to track the true solution perfectly down to near $T_9 = 4$. That interval, $6.4 > T_9 > 4.0$, constitutes the QSE phase of the expansion. For T below 4, the alpha particles remaining cannot be captured fast enough to maintain QSE, however, so that QSE breaks down below $T_9 = 4$ and "freezeout" begins.

is the long-dashed curve, and the QSE solution is the dotted curve. The NSE X_α tracks that of the network quite well from $T_9 = 10$ down to $T_9 \approx 6.4$. This is the NSE phase of the expansion. From this temperature on, the network and NSE alpha mass fractions diverge. This is due to the fact that the reactions assembling heavy nuclei from alpha particles are no longer fast enough to meet the demands of NSE. Although the matter diverges from NSE below $T_9 \approx 6.4$, it remains in QSE. This QSE phase lasts down to $T_9 \approx 4$, as shown by the fact that the QSE and network X_α's track each other down to this temperature. Finally, below $T_9 \approx 4$, the individual nuclear reactions are not fast enough to maintain the QSE. The single, large QSE cluster breaks down into a growing number of smaller QSE clusters. Eventually these break down and the final freezeout occurs.

A key aspect of Figure 3 must be grasped: namely, the abundance X_α is determined by a balance between the capture of alpha particles by the heavy nuclei and their ejection from heavy nuclei. That steady state depends on the number of heavy nuclei and their properties. The abundance X_α is not to be thought of as "an uncaptured residual of the initial excess." From the time that NSE is established (10^{-6} s) until freezeout begins ($T_9 \approx 4$), this steady state is maintained by very fast reactions. If there were no expansion and cooling on a much longer timescale and if there were no change in the number of heavy nuclei also on a much longer timescale, the value of X_α at $T_9 = 5$ (for example) would remain fixed at the value shown in Figure 3. The much slower cooling decreases the photoejection rates of alpha particles and nucleons, so their free densities slowly evolve their quasi-stationary values. This well-known property of NSE also applies to QSE, as first formulated in the simpler process of silicon burning (Bodansky et al. 1968). The difference between the NSE and the QSE distributions is to be found in the number of heavy nuclei Y_h that are maintaining this quasi-steady value of X_α. During the NSE phase, that number Y_h is in equilibrium with the number of alpha particles; but during the QSE phase, that equilibrium is not maintained, and the number of heavy nuclei (in this particular case) is too few to satisfy NSE. We demonstrate this in the next paragraph. But the free alpha density during the QSE phase nonetheless remains in balance between the rates of captures and ejections by whatever heavy nuclei Y_h do exist. It is only during the "freezeout" ($T_9 < 4$) that the quasi-stationary nature of X_α breaks down, after which the remaining alpha particles become potentially capable of capture by the heavy nuclei. And it is only during that final freezeout phase that the abundances change by capturing some of the remaining particles. Furthermore, these same considerations also apply to the free densities of nucleons, as we display below. But first examine the crucial change in the nature of Y_h. It governs the evolution.

The shift to QSE from NSE occurs because the reactions assembling heavy nuclei become too slow. This is evident in Figure 4, which shows Y_h in the expansion. Below $T_9 \approx 6.4$, the network expansion comes to have too few nuclei relative to the number that would be present in the corresponding NSE. The quantity Y_h freezes out in the expansion at $T_9 \approx 5$. This is the temperature at which the $\alpha + \alpha + n \rightarrow {}^9\mathrm{Be}$ then ${}^9\mathrm{Be}(\alpha, n){}^{12}\mathrm{C}$ reaction sequence freezes out. Below $T_9 = 5$, then, the expansion is characterized by a constant Y_h. The value of Y_h for the QSE is never different from that in the network because the QSE is always computed from the instantaneous Y_h in the network.

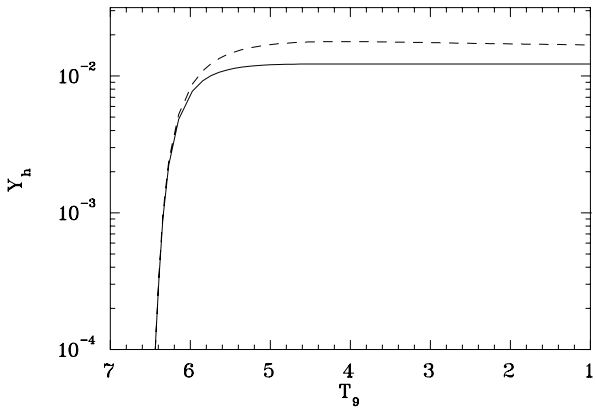

FIG. 4.—Total number of heavy nuclei (C and greater) Y_h in the reference calculation. Y_h rises rapidly as the temperature falls, giving nuclei more stability. The true network solution and NSE values are in agreement from the earliest microseconds (not displayed) down to $T_9 = 6.4$, where NSE begins to break down (see Fig. 3). The sense of this breakdown is here that the network is unable to create enough nuclei to satisfy the expectations of NSE at lower T. The true Y_h levels off early to an asymptotic value. This situation is typical of high-entropy (high-ϕ) expansions. The QSE value of Y_h is exactly satisfied by definition, because the network solution for Y_h is used to compute the QSE distribution (eq. [27]). Understanding the evolution below $T_9 = 6.4$ becomes a matter of reliably calculating the value of Y_h.

Figure 5 shows the average atomic number $\langle Z \rangle$ and average mass $\langle A \rangle$ of heavy nuclei in the network expansion, NSE, and QSE. The NSE and network $\langle Z \rangle$ and $\langle A \rangle$ track each other well down to $T_9 \approx 6.4$, at which point the network abundances are no longer in NSE. From this point

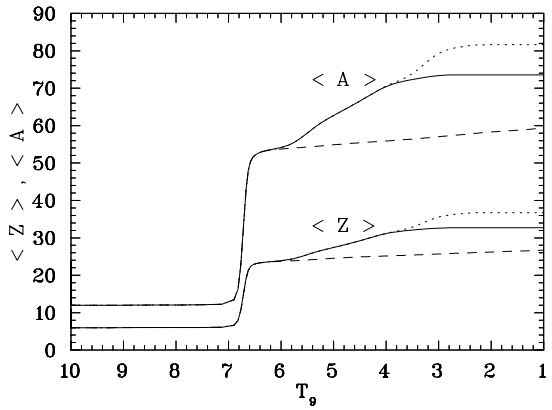

FIG. 5.—Average atomic weight $\langle A \rangle$ and average atomic number $\langle Z \rangle$ of heavy nuclei (C and greater) in the reference calculation. Both rise rapidly as the temperature falls below $T_9 = 7$, giving heavier nuclei increasingly competitive stability. The true network solution and NSE values are in agreement from the earliest microseconds down to $T_9 = 6.4$, where NSE begins to break down (see Figs. 3 and 4). The "true solution," as given by the complete nuclear network, is shown as the solid curve. The average Z and A in NSE at each T is again shown as the long-dashed curve, and the QSE values are shown as the dotted curve. The QSE solution adopts the true Y_h (Fig. 4) and apportions that number among isotopes according to eq. (27). All three solutions are in exact agreement after the first microsecond down to $T_9 = 6.4$ ($t = 0.226$ s). As T_9 falls below 6.4, $\langle A \rangle$ and $\langle Z \rangle$ begin to exceed NSE expectations by increasingly large amounts, marking the breakdown of NSE. The QSE solution, however, continues to track the true solution perfectly down to near $T_9 = 4$. That interval, $6.4 > T_9 > 4.0$, constitutes the QSE phase of the expansion. At lower T, during freezeout, the nuclei would like to be still more massive, but the reactions remaining are inadequate to maintain the QSE. This figure shows that the average size of heavy nuclei is well predicted by the QSE at the freezeout temperature $T_9 = 4$ because the freezeout reactions are unable to change it. Only certain individual nuclei are altered during freezeout.

on, the nuclei in the network are larger on average than those in the corresponding NSE. This is because in the network expansion there are fewer heavy nuclei than in NSE, and they are in the presence of an overabundance of light particles relative to NSE. This shifts the abundances toward heavier mass as prescribed by the still valid QSE. The network abundances eventually diverge from QSE. At low temperature, the average charge and mass of the QSE nuclei become greater than for the network nuclei. In this phase of the expansion, commonly called the freezeout, the nuclear reactions that increase $\langle Z \rangle$ and $\langle A \rangle$ become too slow, thereby preventing the network from keeping up with the QSE. Note, however, that the mean heavy nucleus hardly changes at all during the remaining time; only the unreachable expectations of QSE change as the temperature falls.

Figure 6 shows μ_h/kT during the expansion. Its deviation from zero measures the divergence of the QSE from the NSE. The chemical potential remains accurately $\mu_h/kT = 0$ down to $T_9 \approx 6.4$, confirming that this is the NSE phase. Below this temperature, however, the chemical potential of the heavy nuclei, that is, the free energy "cost" of adding another heavy nucleus, becomes increasingly negative. The system strongly favors any transformation that would decrease its free energy, so it strongly favors adding another heavy nucleus. The problem is that the timescale to do this is too long. As the expansion continues, the number of heavy nuclei diverges even further from that demanded by NSE, so the potential gain to the system by adding heavy nuclei becomes even greater. At the same time, however, the timescale to assemble heavy nuclei becomes even longer. From this energetics point of view, the network expansion vastly differs from NSE at $T_9 \approx 4$, the end of the QSE phase.

Figure 7 shows the mass fractions of neutrons and protons during the expansion compared to their NSE and QSE values. In agreement with the other diagnostics of this expansion, we see that NSE is maintained in the network down to $T_9 \approx 6.4$, and QSE is maintained down to $T_9 \approx 4$.

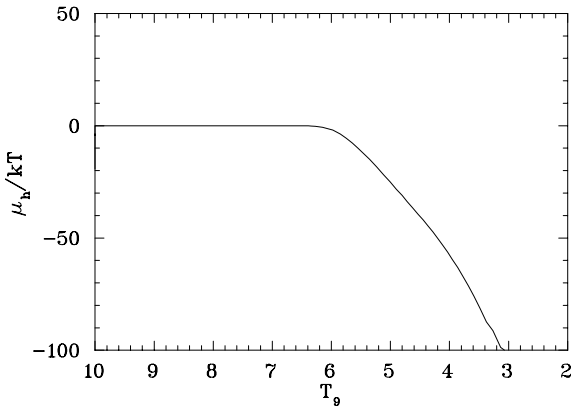

FIG. 6.—Chemical potential of the heavy nuclei (which exist in QSE above $T_9 = 4$) as temperature falls during the reference calculation. Down to almost $T_9 = 6$, that value is $\mu_h = 0$, which is appropriate for the NSE. After NSE breaks down at $T_9 = 6.4$, however, the value of μ_h becomes increasingly negative. "Negative cost" for assembly of a heavy nucleus means that during that QSE phase, the distribution would welcome more nuclei on energetic grounds; however, the inability to rapidly increase Y_h constrains the solution to the QSE distribution. As T declines, the energetic distance of the QSE from the NSE continues to grow. This reflects the increasing importance of the Lagrangian constraint λ_h in eq. (26) and the subsequent variational statement (eq. [25]). The decline of the free energy (eq. [25]) is throttled by constriction in the rate of growth of Y_h.

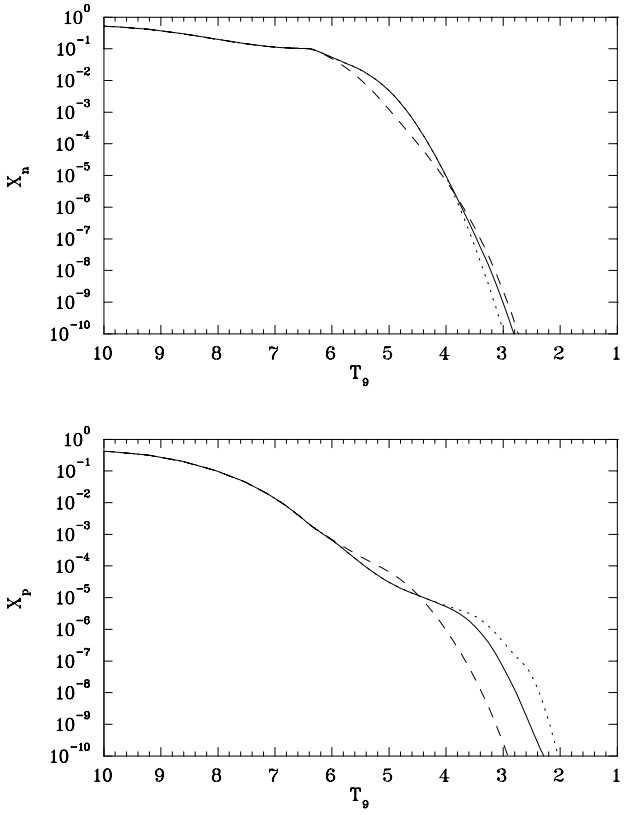

FIG. 7.—Mass fractions of free nucleons in the reference expansion are compared with their NSE (*long-dashed curve*) and QSE (*dotted curve*) values. The QSE values take the value of Y_h from the network calculation. Long after the NSE has broken down, it just happens that the free NSE densities pass through the true densities as the QSE approaches freezeout. That coincidence does not place the assembly near NSE; indeed, the alpha-particle density (Fig. 3) is very far from NSE at that time, as is the heavy element distribution. Other curious features, such as the NSE and QSE solutions lying on opposite sides from the true solution, are understandable.

These free nucleons are maintained by a quasi-stationary balance between capture and ejection by the heavy nuclei, just as in the case of X_α in Figure 3. This explains why both X_n and X_p approach values near 10^{-5} at freezeout. The binding energies of protons and neutrons are nearly equal in the dominant heavy nuclei (e.g., ^{62}Ni).

Of perhaps even greater interest is the question of the equilibrium among neutrons, protons, and alpha particles. Figure 8 shows the quantity $R = R_\alpha R_n^{-2} R_p^{-2}$ as a function of the temperature during the expansion. This ratio R is not to be confused with $R_\alpha = Y_\alpha/Y_\alpha^{\rm NSE}$. R measures how well the neutrons and protons are in equilibrium with the alpha particles. A strict QSE requires that R be unity, which it is in this expansion down to the freezeout of the equilibrium among the neutrons, protons, and alpha particles beginning at $T_9 \approx 3.4$. The equality $R = 1$ is maintained by numerous fast reaction cycles of the form ^{62}Ni$(p, \gamma)^{63}$Cu$(n, \gamma)^{64}$Cu$(n, \gamma)^{65}$Cu $(p, \alpha)^{62}$Ni and their inverses. Below $T_9 \approx 3.4$, those cycles become too slow in their consumption of alpha particles. At temperatures immediately below $T_9 = 3.4$, therefore, the system comes to have too many alpha particles.

We turn finally to the abundances of heavy nuclei in the expansion. Figure 9 shows $X(^{62}\text{Ni})$, the mass fraction of ^{62}Ni in the network expansion compared to the corresponding NSE and QSE values. ^{62}Ni is, after the alpha

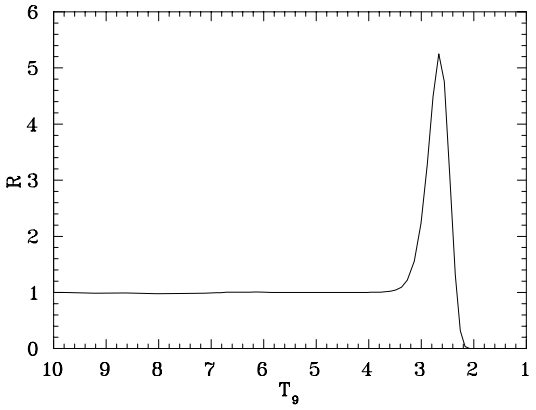

FIG. 8.—Quasi-equilibrium among the densities of free protons, neutrons, and alpha particles is measured by the ratio $R = R_\alpha R_p^{-2} R_n^{-2}$. When $R = 1$, the reactions converting nucleons to alpha particles proceed at the same rate as the reactions converting alpha particles to nucleons. This relates their QSE densities. This aspect of QSE is maintained accurately down to $T_9 = 3.4$, below the breakdown of the QSE by other measures of it. One consequence of this balance of rates in QSE is that all free particles contribute equally to the evolution of abundance distributions, so that no class of reactions can be singled out as carrying the flow.

particles, the most abundant species at the end of this particular calculation. Its network abundance is well tracked by NSE down to $T_9 \approx 6.4$ and by QSE down to $T_9 \approx 4$, in agreement with the previous diagnostics. An important semantic point attends the increasingly large excess of ^{62}Ni over its NSE value during the temperature decline from $T_9 = 6$ to $T_9 = 4$. One sometimes hears this attributed to "capture of alpha particles" by the NSE distribution; but that is incorrect. That hump reflects the evolution of the

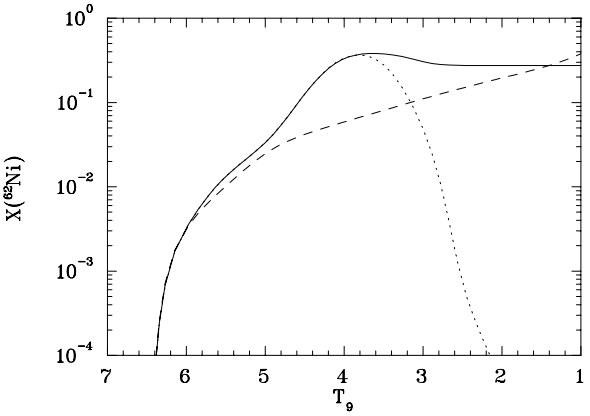

FIG. 9.—Evolution of the abundance by mass fraction of one significant nucleus, ^{62}Ni, during the reference expansion. The solid curve again represents the true solution, with the long-dashed and dotted curves representing, respectively, the NSE and QSE abundance. The QSE abundance adopts the true value for Y_h. This abundant nucleus represents more than 10% of the matter as the QSE approaches freezeout. The NSE abundance fails badly, but the QSE abundance is accurate down to $T_9 = 3.8$. Quite evidently, the true final abundance of this and other abundant nuclei are well represented by their QSE abundances near freezeout, $T_9 = 4$. This huge QSE distortion of the abundance was discovered by Meyer et al. (1996), who showed (their Fig. 3) just the opposite distortion for ^{48}Ca as that seen here for ^{62}Ni. At a time when the NSE distribution shows large quantities of both ^{48}Ca and ^{62}Ni, the QSE in the presence of an excess of light particles (relative to NSE) shifts the ^{48}Ca mass downward while it drives the ^{62}Ni mass upward (shown here).

QSE. The QSE value of $X(^{62}\mathrm{Ni})$ later falls precipitously away from the true solution below $T_9 \approx 4$. This happens because the QSE abundance distribution shifts to even higher mass nuclei. Of course, in this freezeout phase, the network cannot keep up, and the actual ^{62}Ni mass fraction drops by only $\sim 40\%$ before it freezes out. Interestingly, the NSE mass fraction of ^{62}Ni eventually surpasses that of the network for very low temperature. This reflects the fact that this isotope is among the most strongly bound isotopes with the Y_e of the system at those conditions, so it becomes increasingly favored in NSE as the temperature declines further. This point, however, is not physically relevant because during the dynamic expansion, NSE became a poor description of the actual abundances long before these low temperatures were reached. Of much greater physical relevance is the question of the modification of the QSE abundances during freezeout. The QSE abundances at the beginning of freezeout ($T_9 = 4$) give the actual final abundance to $\sim 40\%$ accuracy. Admittedly, higher entropy or neutron richness would lead to less accuracy because of greater freezeout modifications. Nevertheless, factor of 2 accuracy is often sufficient for many applications, and there is a possibility that useful estimates of abundance yields from QSE freezeouts can be easily made if we have a reasonable guess for Y_h. We return to this question in § 5.

As a final consideration, we present the evolution of the elemental abundance distribution during the expansion in Figure 10. At $T_9 = 5.85$, the network and NSE abundances have only begun to diverge. The dotted QSE curve overlaps the network solution and cannot be seen. By $T_9 = 4.03$, nearing the end of the QSE phase of the expansion, however, the network and NSE abundances are greatly different, with the network abundances dominated by much larger nuclei than NSE. The QSE abundances remain exactly correct within the accuracy of this figure and still do not show up independently. Notice especially the huge secondary Sr peak, which is correctly given by QSE but totally absent in NSE. By $T_9 = 3.84$, the network is no longer able to keep up with the QSE. The nuclei in QSE ask to have slightly larger charges on average than nuclei in the network, but the reaction rates can no longer oblige. By $T_9 = 2.08$, the network abundance distribution has frozen out with nuclei lower in charge on average than those in QSE; but the QSE is no longer physically relevant at that low temperature. This in fact was already evident in Figure 5.

The panels of Figure 10 reveal the emergence of order from disorder. They demonstrate a system finding its own rules for establishing order. Order appears as a residual imposed by the twin temporal evolutions, expansion and cooling. The self-organization of populations into ordered arrays in the face of complex circumstances again calls to mind the quotation from Kauffman (1995) given in the Introduction (§ 1). To grasp the point most easily, we ask the reader to examine the Sr abundance peak that has emerged in the $T_9 = 4.03$ panel of Figure 10 and that remains to the end. Such a huge abundance peak is totally absent in NSE distributions at all temperatures. Recall in this regard that NSE abundances are disordered abundances. An NSE distribution is maximally disorganized thermostatistically, analogous to maximal disordering of the Maxwell-Bolzmann distribution of ion velocities. NSE disorder exists initially in our calculations, but by $T_9 = 4.03$ it has disappeared, and the new population includes the

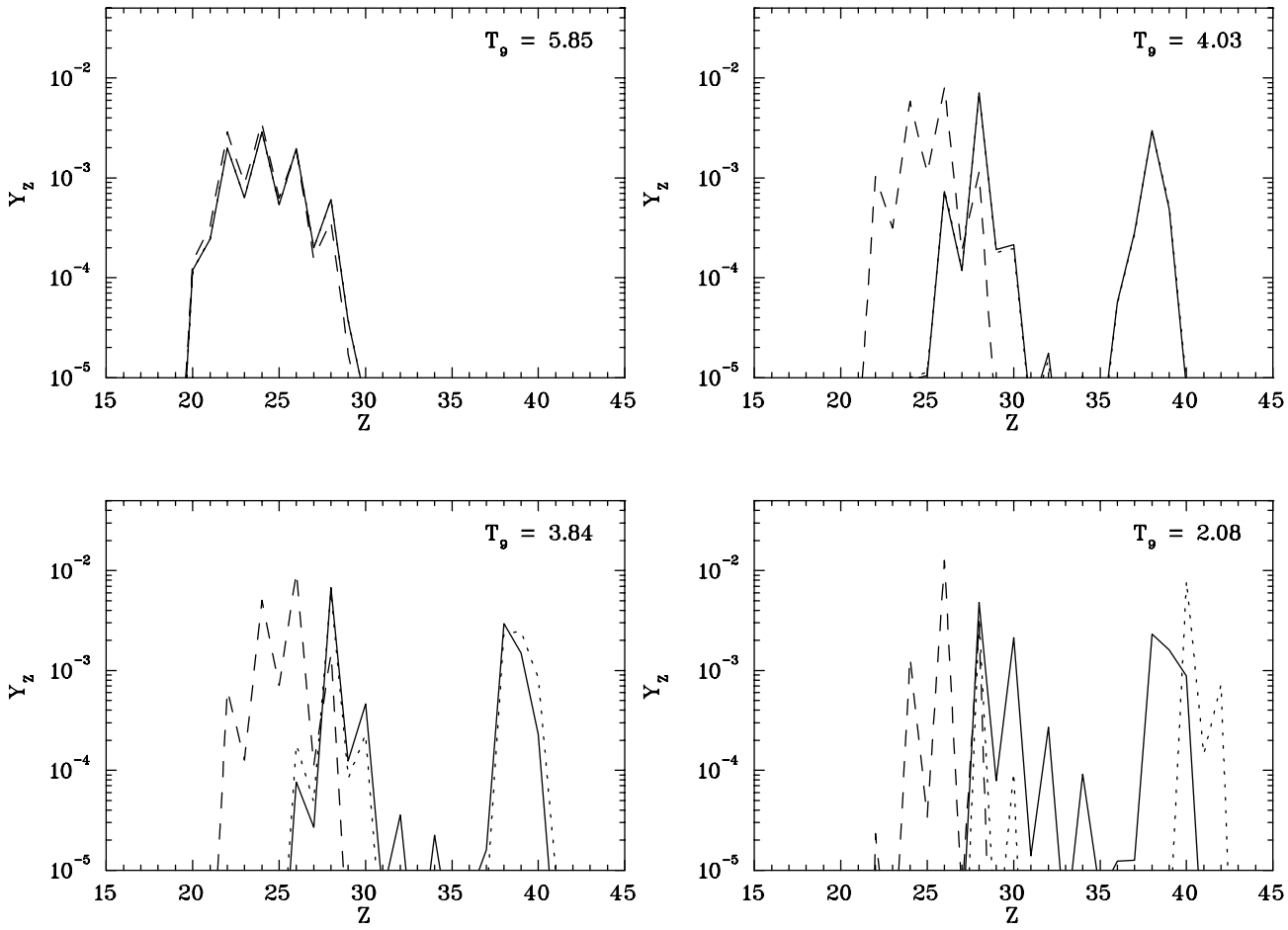

FIG. 10.—Comparison of the true heavy-element abundance distribution with the NSE (*long-dashed curves*) and the QSE (*dotted curves*) distributions within the reference expansion are shown. At $T_9 = 5.85$, the NSE distribution has just deviated noticeably from the true distribution for the first time. The QSE distribution cannot be seen because it overlaps the true distribution perfectly. This time lies squarely in the QSE regime (see Figs. 3, 4, and 5). The true distribution has begun to have more of the most massive nuclei shown and fewer of the least massive ones, a trend that subsequently intensifies. At $T_9 = 4.03$, the NSE distribution deviates greatly from the true one, whereas the QSE solution is still so exact that it cannot be seen atop the true distribution. Not only are the heavy nuclei much heavier than the NSE mean, but an entire secondary peak at $Z = 38$ has appeared. Even though the freezeout of the QSE is about to begin, its solution is exact at this time. At $T_9 = 3.84$, the QSE distribution has just deviated noticeably from the true one for the first time. Freezeout has begun, and the abundances are close to their final values. QSE is a good estimator of the abundance distribution. At $T_9 = 2.08$, the abundance distribution is essentially frozen and differs in only subtle ways from that at $T_9 = 3.84$; viz., the $Z = 30$ subpeak came up relative to the main nickel peak; the $Z = 32$ and 34 subpeaks came up even more, owing to freezeout capture of free light particles; and the Sr peak squared up a bit owing to freezeout captures predominantly of protons. The QSE distribution (*short-dashed curve*) at this temperature is now quite irrelevant, fitting poorly, because the freezeout reactions cannot keep pace with QSE's demands. NSE is even more irrelevant.

persistent Sr peak. The $T_9 = 4.03$ panel distribution differs greatly from the long dashes, which show NSE's disorder. The Sr peak displays order also according to the common usage. Those nuclei are not broadly spread out but stand together at $Z = 38$, 39, 40 like Stonehenge bluestones. It would be as if the nearly Maxwellian ion energies were accompanied by a hugely overpopulated group at, say, 3.8–4.0 kT!

We speak allegorically not out of poetic license but for the sake of communicating the sense in which order appears. It is the QSE concept and its Y_h governor that enable us to comprehend that evolutionary emergence. Additional order appears as that QSE in turn freezes out, such as the large increase in the $Z = 30$, 32, 34 nuclei relative to the $Z = 28$ maximum during the transition from $T_9 = 3.84$–2.08, when QSE has itself broken down and additional constraints appear on the free energy minimum. Indeed, for even larger values of entropy and neutron richness, the extra layer of order emerging from QSE breakdown is no less than the ordered heavy nuclei of the *r*-process.

3.4. *Other Expansions*

The reference expansion presented in the previous subsection illustrated many of the key points surrounding QSE nucleosynthesis. Nevertheless, we gain further insight by also considering the results of our eight other expansions calculated with differing initial combinations of η_0 and ϕ. Our nine survey expansions utilized $\eta_0 = (0.03, 0.10, 0.1667)$ and $\phi = (1.7, 6.8, 17)$.

Figure 11 shows the evolution of Y_h for all nine expansions. In this figure, each panel shows the results for given ϕ (as labeled) but with $\eta_0 = 0.03$ (*solid curve*), $\eta_0 = 0.10$ (*dashed curve*), and $\eta_0 = 0.1667$ (*dotted curve*). Comparison of the three panels makes one point clear: lower ϕ expansions produce more heavy nuclei. This is a consequence of

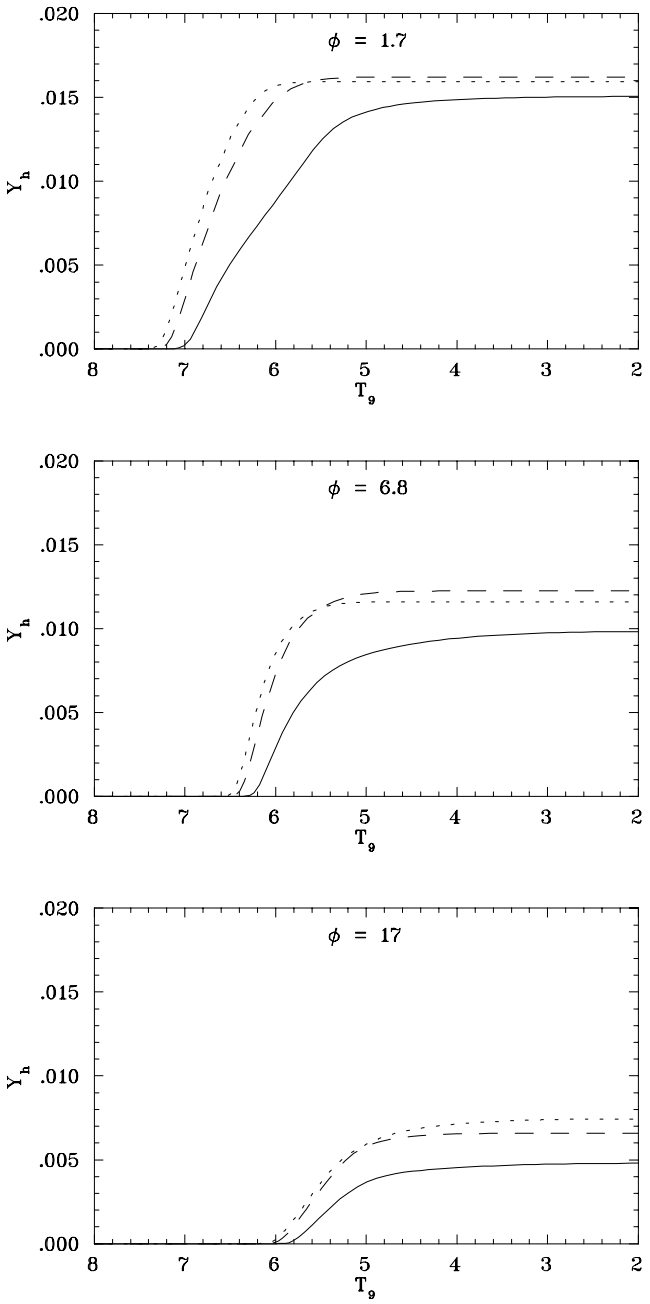

FIG. 11.—Abundance of heavy nuclei during each of the nine expansions. The line types are for $\eta_0 = 0.03$ (*solid curve*), $\eta_0 = 0.1000$ (*dashed curve*), and $\eta_0 = 0.1667$ (*dotted curve*). Lower ϕ expansions produce more heavy nuclei. Lower ϕ means that the NSE shift from an abundance distribution favoring light particles to one favoring heavy nuclei occurs at a higher temperature. A lower ϕ also means the density is higher and, consequently, the three-body reactions assembling heavy nuclei are more rapid for a given temperature. Also, more neutron-rich expansions tend to make more nuclei because of the greater efficacy of the reaction sequence through ^{9}Be. The $\eta_0 = 0.1667$ expansions typically make fewer heavy nuclei than the $\eta_0 = 0.1000$ expansions. This is deceptive, however, because the mass of the heavy nuclei in former expansions is greater (see Fig. 12). This translates into a greater *mass fraction* in heavy nuclei for the $\eta_0 = 0.1667$ expansions.

two effects. First, the NSE shift from an abundance distribution favoring light nuclei (n, p, α) to one favoring heavy nuclei occurs at higher temperature for lower ϕ. Because ϕ is the number of photons per nucleon, the larger is ϕ for a given density, the greater is the temperature and the associated photodisintegration rate of nuclei and, consequently, the lower is the abundance of heavy nuclei. A later shift to heavy nuclei will give the system less time to assemble heavy nuclei. Second, larger ϕ corresponds to a lower density for a given temperature. Because the three-body reactions that assemble heavy nuclei have timescales $\propto \rho^{-2}$, larger ϕ's correspond to slower reactions assembling heavy nuclei and thus to production of fewer heavy nuclei. These nucleosynthesis effects are analogous to recombination of ionized hydrogen. Larger ϕ expansions would produce more light particles (electrons) because the equilibrium shift from ions and electrons to neutral atoms occurs at lower temperature than for smaller ϕ, and, once the shift takes place, larger ϕ means a lower density and a lower recombination rate.

Other aspects of Figure 11 deserve comment. Larger η_0 yields more heavy nuclei. More neutron-rich systems utilize a more efficacious reaction sequence $\alpha + \alpha + n \rightarrow {}^9\mathrm{Be}$ followed by ${}^9\mathrm{Be}(\alpha, n){}^{12}\mathrm{C}$. This sequence allows more of the mass to assemble into heavy nuclei than could be achieved by triple-α alone. It does not follow, however, that larger η_0 necessarily yields more heavy nuclei. Although the solid curve yields the smallest Y_h in each panel, the largest η does not always yield the greatest Y_h. This is evident in the $\phi = 6.8$ panel. Here the $\eta_0 = 0.1667$ expansion ended up with fewer heavy nuclei ($Y_h = 1.16 \times 10^{-2}$) than the $\eta_0 = 0.10$ expansion ($Y_h = 1.23 \times 10^{-2}$). The nuclei in the $\eta_0 = 0.1667$ expansion, however, were considerably larger ($\langle A \rangle = 85.8$) than those in the $\eta_0 = 0.10$ expansion ($\langle A \rangle = 73.6$), as evident from Figure 12. Therefore, the $\eta_0 = 0.1667$ expansion yielded a larger mass fraction X_h of heavy nuclei ($X_h = 0.995$) than the $\eta_0 = 0.10$ expansion ($X_h = 0.905$). Increased neutron richness especially helps the rate of growth of Y_h at early time, as is visible in all three panels above $T_9 = 6$. A final aspect of Figure 11 is that Y_h continues to grow slowly for some of the expansions, at least down to $T_9 = 2$. This is especially evident for the $\phi = 6.8$, $\eta_0 = 0.03$ and the $\phi = 17$, $\eta_0 = 0.1667$ expansions. The former expansion has such a large number of free alpha particles at low temperature that the triple-α reaction continues at a nonnegligible rate. For the latter expansion, a large number of free alpha particles and neutrons is present at low temperature, so the reaction sequence through ^{9}Be continues.

Figure 12 shows the evolution of the average atomic number $\langle Z \rangle$ and average mass number $\langle A \rangle$ of the heavy nuclei for all nine expansions. The line types in each panel indicate the neutron richness of each expansion, as in Figure 11. From this figure it is evident that for given η_0, larger ϕ expansions give larger nuclei. The QSE concept explains that, simply, larger ϕ corresponds to a greater abundance of free nucleons, which shifts the QSE abundances to greater mass.

Also noteworthy in Figure 12 is the increase with η_0 of the average mass of nuclei for each ϕ. This important feature for supernova nucleosynthesis was first recognized by Woosley & Hoffman (1992). As we discuss in more detail in § 4, however, their explanation of this in terms of (α, n)-reactions carrying flow to higher mass is misleading. The more correct explanation relies on the QSE nature of the expansions and the underlying nuclear physics. Figure 13 shows the binding energy per nucleon of the most bound isotope for each element in three different ranges of neutron richness in the nucleus. It is important to note that η in this

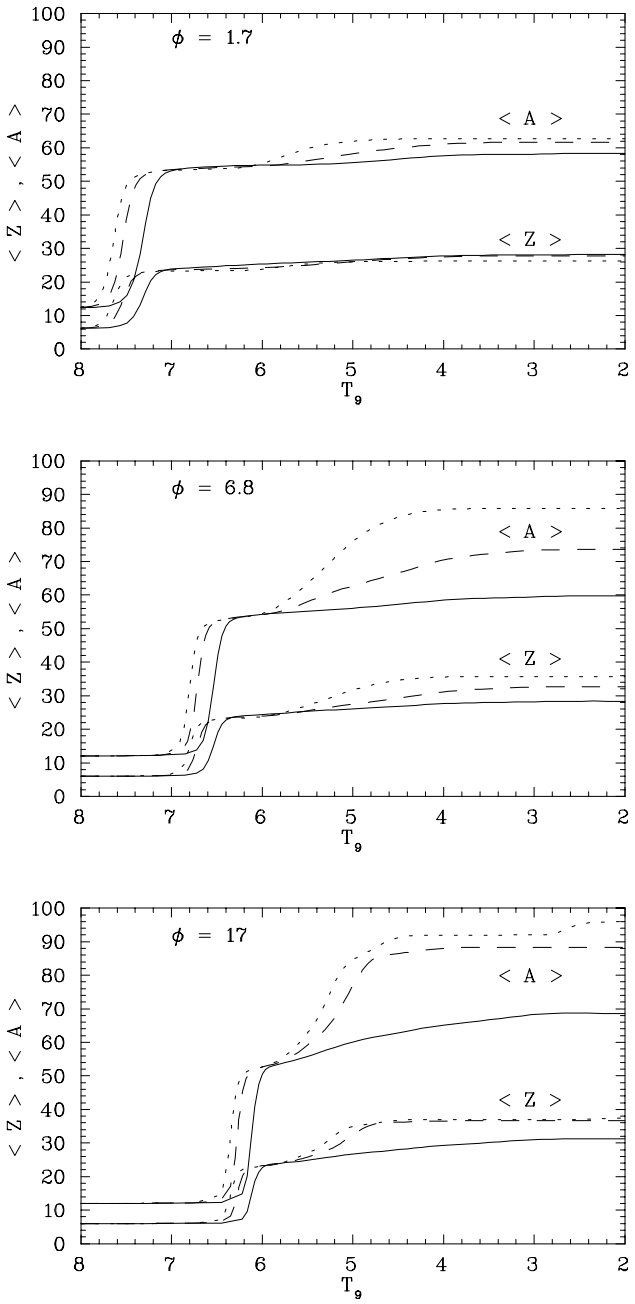

FIG. 12.—Average atomic number ($\langle Z \rangle$) and mass number ($\langle A \rangle$) during each of the nine expansions. As in Fig. 11, the line types are for $\eta_0 = 0.03$ (*solid curve*), $\eta_0 = 0.1000$ (*dashed curve*), and $\eta_0 = 0.1667$ (*dotted curve*). Larger ϕ expansions tend to produce larger nuclei. In the QSE phases of these expansions, the nuclei are in the presence of an excess (relative to NSE) of light particles. This tends to shift the nuclei upward in mass. Also clear is the fact that more neutron-rich expansions produce larger nuclei. For nuclei with small neutron excesses, iron-group nuclei are more fit in competing for abundance in equilibrium because of their strong nuclear binding. This "fitness" advantage lessens as the neutron excess of the nuclei grows (see Fig. 13). For this reason, large-mass nuclei compete favorably for abundance in neutron-rich expansions. Notice the mini–*r*-process occurring at the end of the $\phi = 17$, $\eta_0 = 0.1667$ expansion leading to an increase in the average mass number as T_9 drops below 3.

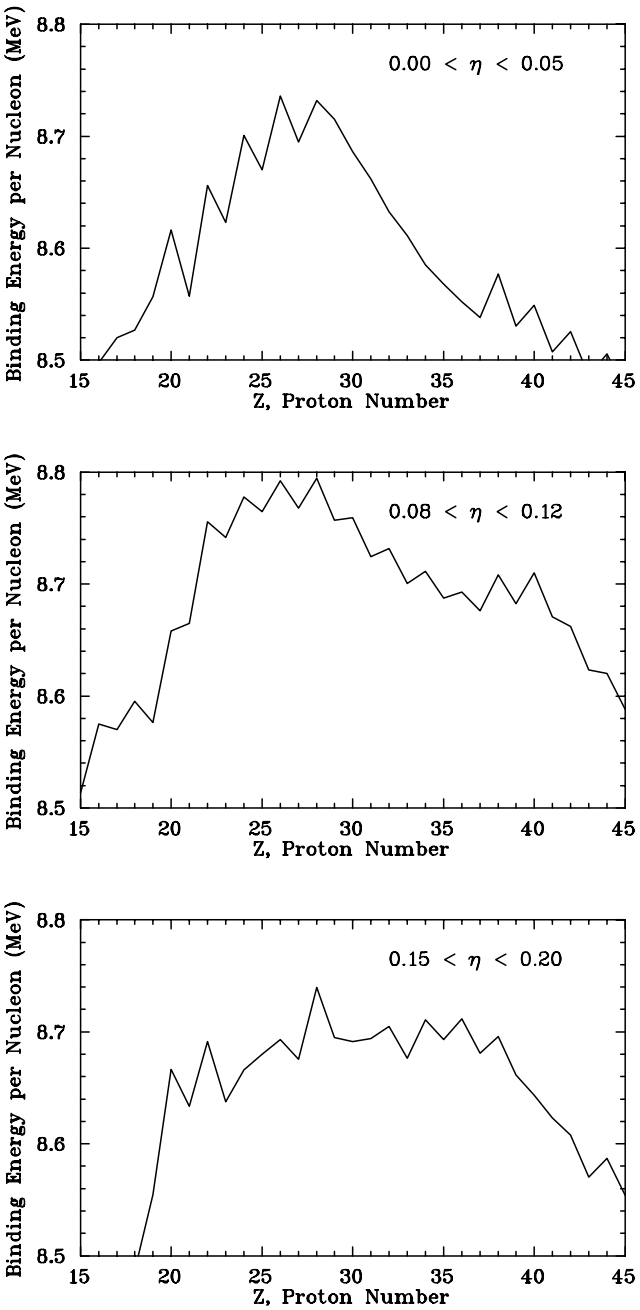

FIG. 13.—Binding energy per nucleon for isotopes whose neutron excess (i.e., nuclear η) lies in the indicated range. Only the most tightly bound isotope in the given nuclear η range for each element is shown. For isotopes with neutron excesses between 0.00 and 0.05, Fe and Ni isotopes dominate the binding energy per nucleon curve. That is why these isotopes dominate the equilibrium abundance for low-η expansions, no matter what the entropy. For increasing nuclear η, isotopes of elements with $Z = 35$–40 have binding energies per nucleon comparable to those of the Fe and Ni. That is why these nuclei compete effectively for abundance in QSE in neutron-rich expansions.

figure is not the neutron richness of the system but rather $(N - Z)/A$ for each isotope. For isotopes with $\eta = (N - Z)/A$ in the range $0.0 < \eta < 0.05$, the maximum binding is sharply peaked around ^{54}Fe and ^{58}Ni. Isotopes with $Z \approx 40$ are more than 0.1 MeV per nucleon less bound than those Fe and Ni isotopes. For example, ^{80}Sr is 0.16 MeV per nucleon less bound than ^{54}Fe. As we look at more neutron-rich nuclei, however, the $Z \approx 40$ isotopes become more tightly bound relative to the Fe and Ni isotopes. For $0.08 < \eta < 0.12$ nuclei, ^{90}Zr is only 0.074 MeV per nucleon less bound than ^{62}Ni, the most bound isotope in this η

range. For $0.15 < \eta < 0.20$ nuclei, ^{86}Kr is only 0.028 MeV per nucleon less bound than ^{66}Ni, the most bound isotope for this η range. The consequence of this nuclear fact is that, in a QSE, elements with $Z = 35$–40 can compete favorably with those in the $Z = 26$–30 range if the system is neutron rich enough to have large η isotopes present.

Before leaving Figure 12, we note the behavior of $\langle A \rangle$ for the $\phi = 17$, $\eta_0 = 0.1667$ expansion at low temperature. The rise near $T_9 = 5$ represents the QSE establishment of the "Sr peak," as in Figure 10. As T_9 drops below 2.7, moreover, $\langle A \rangle$ rises again by about five or six units. This is a brief *r*-process phase of this expansion. The reduced density of thermal gamma rays allows a final flurry of neutron captures, with little associated increase in $\langle Z \rangle$ by β^- decay. At $T_9 = 2.7$, $Y_n/Y_h = 5.53$, so each nucleus captures on average roughly five neutrons during the final freezeout. A more extreme entropy or neutron richness would lead to a larger neutron-to-seed ratio and a more robust *r*-process.

Figure 14 shows the elemental abundances for all nine of the expansions at a common reference temperature, $T_9 = 4.5$, a point late in the QSE phase of each expansion. These abundance distributions were calculated with the full reaction network; however, they also match the QSE distribution well, as was demonstrated in Figure 10. They reflect the underlying nuclear physics already illustrated in Figure 13. As in Figures 11 and 12, the line type indicates the initial neutron richness of the expansion. First we call attention to the fact that for all three ϕ's, the $\eta_0 = 0.03$ abundance distribution is always peaked in the Fe-Ni region. This is true even for $\phi = 17$, although the extreme photon-to-nucleon ratio here gives a sufficiently large abundance of free nucleons that a small abundance peak at Sr appears. For this neutron richness, only isotopes with nuclear η's in the range of the top panel in Figure 13 are highly populated. The sharp peak in the binding energy per nucleon in the Fe-Ni region for isotopes within this range of nuclear η's ensures that only these elements have large abundances in QSE: they have a great "fitness" advantage over other species. For the dashed curves having $\eta_0 = 0.10$, the system is neutron rich enough to allow population of isotopes with larger nuclear η's. Thus, for $\phi = 6.8$ or 17, for which a large enough QSE abundance of free nucleons is present, a significant abundance of these elements builds up. In fact, for $\phi = 17$, the abundance distribution is dominated by Kr. By contrast, the $\phi = 1.7$, $\eta_0 = 0.1667$ expansion does not have enough free nucleons to shift many nuclei from Ni to the Sr region.

For the dotted curves in Figure 14, having $\eta_0 = 0.1667$, we see an extraordinary range of abundance distributions. For $\phi = 1.7$, ^{66}Ni is the most abundant species, and ^{68}Ni comes in second. This is not surprising, since the Ni isotopes are so tightly bound. Remarkably, however, ^{48}Ca is in third. This expansion has a sufficiently low abundance of free nucleons, and ^{48}Ca is only 0.073 MeV per nucleon less bound than ^{66}Ni, that this low-Z species competes favorably with higher Z isotopes. The large ^{48}Ca abundance survives in this expansion because the system ends up with too many nuclei relative to NSE. As discussed in detail in our previous paper (Meyer et al. 1996), this fact points to certain Type Ia supernovae as the source of this isotope. By contrast, the $\phi = 6.8$ abundance distribution is dominated by Kr. This expansion has sufficiently high entropy that at this time it has too few nuclei relative to NSE. The situation is even more extreme for $\phi = 17$. Interestingly, Se ($Z = 34$) and Kr ($Z = 36$) share the abundances roughly equally. This is a surprise, since the less neutron-rich expansion with ($\eta_0 = 0.10$) and $\phi = 17$ has *larger* charge isotopes in the QSE than does $\eta_0 = 0.1667$. It is also perhaps surprising on nuclear grounds; however, it can be understood by the QSE concept and the ways in which the free-particle densities depend upon neutron richness. The $N = 50$ isotones ^{84}Se and ^{86}Kr dominate the elemental abundances. ^{84}Se is 0.053 MeV per nucleon less bound than ^{86}Kr. Nevertheless, ^{84}Se is highly abundant because the $\eta_0 = 0.1667$ expansion is

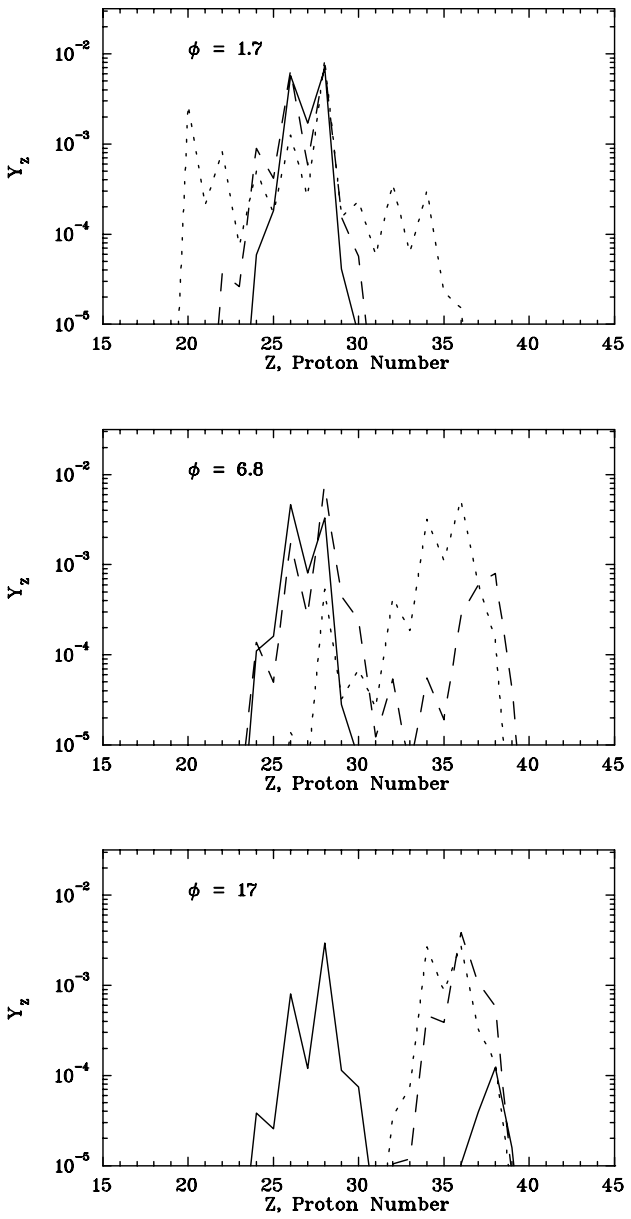

FIG. 14.—Elemental abundances for the nine expansions at $T_9 = 4.5$, a point late in the QSE phase of each expansion. As in Figs. 11 and 12, the line types are for $\eta_0 = 0.03$ (*solid curve*), $\eta_0 = 0.1000$ (*dashed curve*), and $\eta_0 = 0.1667$ (*dotted curve*). For all three ϕ's, the $\eta_0 = 0.03$ expansion abundances are dominated by Fe and Ni. For more neutron-rich expansions, other elements can dominate the abundances. For the low-entropy $\phi = 1.7$, neutron-rich $\eta_0 = 0.1667$ expansion, Ni isotopes dominate, but ^{48}Ca is also highly abundant. This abundant ^{48}Ca survives because the expansion ends with too many nuclei compared to NSE. For larger-ϕ expansions, larger-Z elements can have substantial abundances in QSE if the matter is neutron rich enough (see Fig. 13).

neutron rich and must accommodate more neutron-rich species than the $\eta_0 = 0.10$ expansion. The QSE chooses this distribution over one dominated by more neutron-rich Kr isotopes because of the strong $N = 50$ binding for ^{84}Se.

Figures 15, 16, and 17 show the extent of the QSE at $T_9 = 4.5$ for all nine expansions. Nuclides marked by a circle (open or filled) have a mass fraction greater than 10^{-20} at $T_9 = 4.5$. Filled circles show nuclides in QSE with the most abundant isotope, itself indicated by the intersection of the dotted lines. Our criterion for an isotope i being in QSE with the most abundant species is that $0.9 \leq (Y_i/Y_i^{\rm QSE})/(Y_k/Y_k^{\rm QSE}) \leq 1.1$, where k is the index of the most abundant species, and the QSE abundances are found from equation (27). In all nine cases, the QSE cluster including the most abundant species is large.

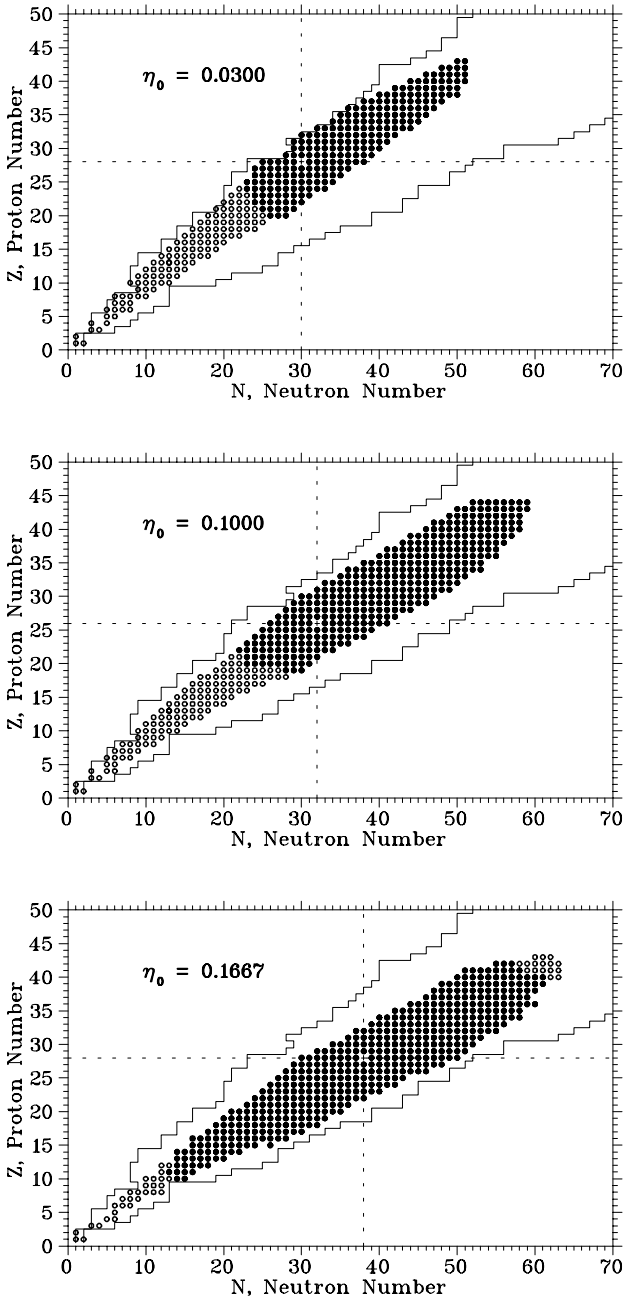

FIG. 15.—Extent of the QSE in the neutron number–proton number plane for $\phi = 1.7$ and the indicated η_0's at $T_9 = 4.5$. The boundaries of the nuclear network are shown as the solid curves. The intersection of the two dotted lines indicates the most abundant heavy isotope. Any nuclide marked by a circle has a mass fraction greater than 10^{-20}. If the circle is filled, that nuclide is in QSE with the most abundant species. The extent of the QSE is large for all three η_0's. The more neutron-rich expansions have clusters shifted to more neutron-rich isotopes to accommodate the greater excess of neutrons. The QSE clusters in the more neutron-rich expansions also are greater in extent in Z, reflecting the more uniform binding energy per nucleon for different elements (see Fig. 13) in neutron-rich systems.

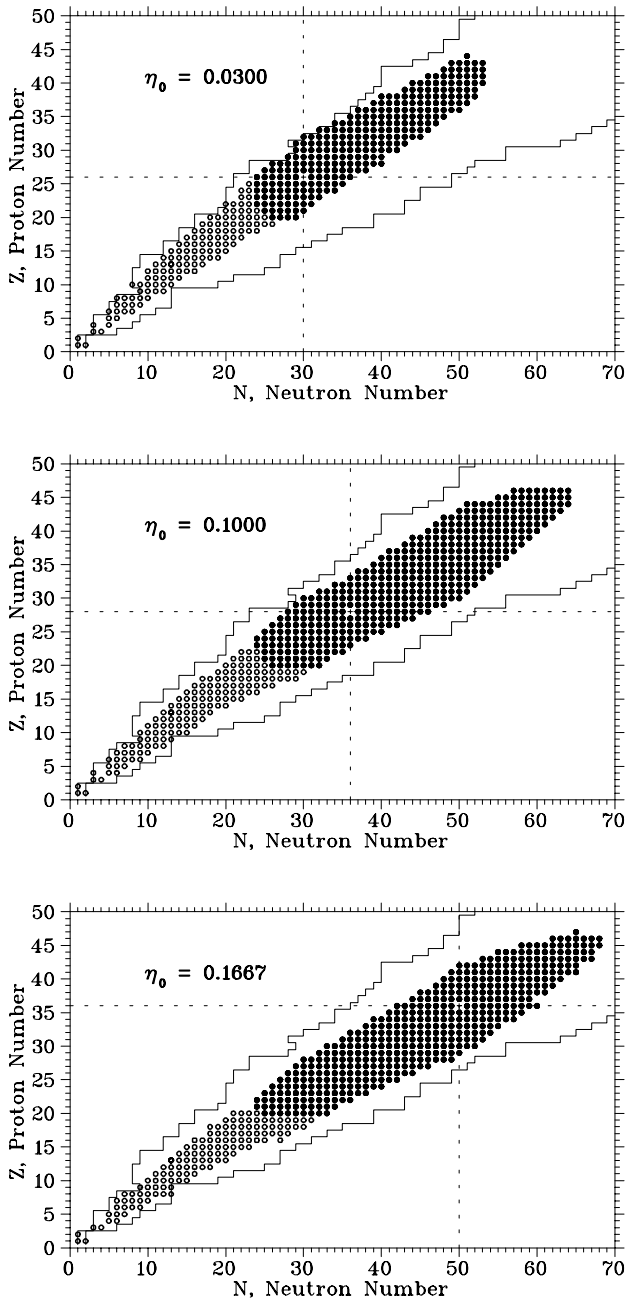

FIG. 16.—Same as Fig. 15, but for $\phi = 6.8$. The general trends in Fig. 15 are also present here. Also noteworthy is the fact that a Kr, rather than a Ni or Fe, isotope dominates the abundance for the $\eta_0 = 0.1667$. This fact was already apparent in Fig. 14 and reflects the strong binding of neutron-rich Kr isotopes relative to comparably neutron-rich Fe and Ni isotopes.

These figures contain three other noteworthy features. First, for given ϕ, a larger η_0 shifts the QSE cluster to more neutron-rich nuclei because the system must accommodate the extra neutrons. Second, for $\phi = 1.7$, the dominant

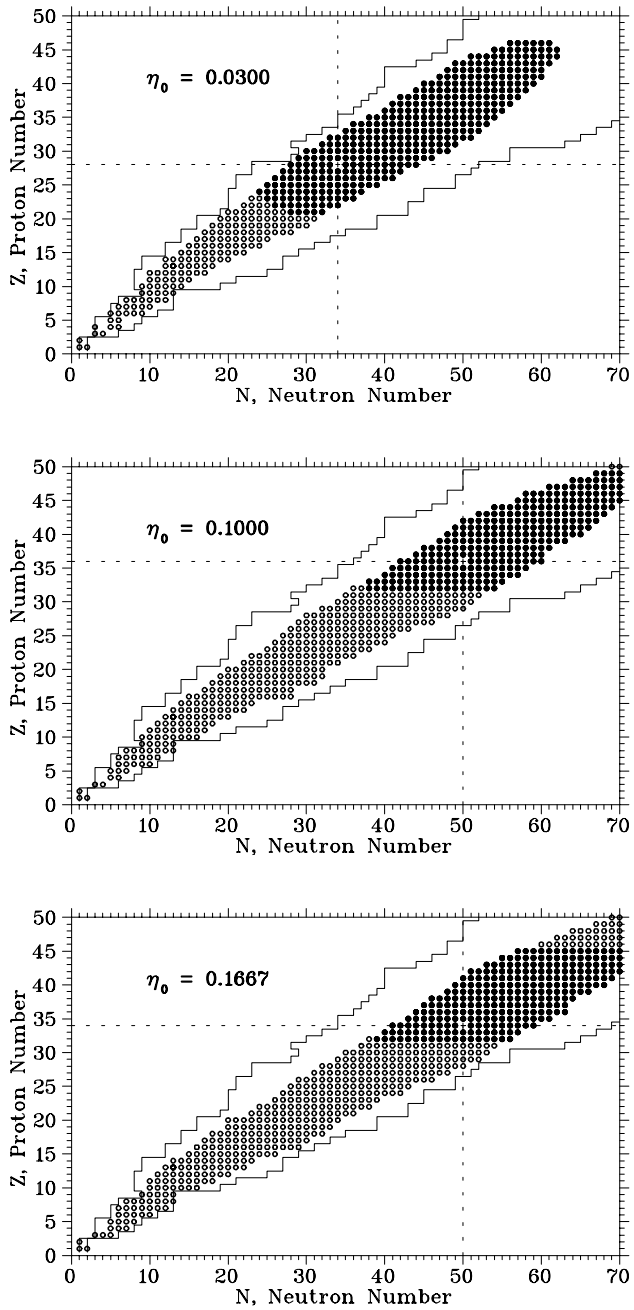

FIG. 17.—Same as Fig. 15, but for $\phi = 17$. Again, the more neutron-rich expansions have QSE clusters shifted to more neutron-rich isotopes. Remarkably, the $\eta_0 = 0.1667$ QSE cluster is rather limited in its extent in Z. This results from the freezing out of the QSE. New heavy nuclei are still forming from the abundant alpha particles and are still moving up to the QSE peak at Se. The nearly divergenceless flow from C to Zn is not as rapid as required by the QSE, however, and the isotopes in that range have become overabundant relative to the QSE (see Fig. 18).

isotope in the QSE cluster is always one of Fe or Ni. For $\phi = 6.8$ or 17, however, the dominant isotope can be a Kr or Se isotope if the matter is neutron rich enough. As previously seen in Figure 13, the greater the nuclear η, the more effectively higher charge elements compete for abundance in QSE, especially when the number of heavy nuclei falls short of that in the corresponding NSE. Third, for $\phi = 1.7$ and 6.8, the greater the neutron richness, the more extensive in Z is the QSE cluster. Again, reference to Figure 13 helps to explain this. The flatness of the binding energy per nucleon versus Z curve for the more neutron-rich nuclei means that there are less severe binding energy differences among these nuclei. This allows reverse reactions carrying nuclei to lower nuclear charge to proceed sufficiently rapidly to maintain the QSE. By contrast, for less neutron-rich nuclei, large nuclear binding occurs over a more limited range of Z, which in turn limits the range of the QSE by restricting the range over which reverse reactions (of any kind) occur sufficiently rapidly.

The exception to this last point occurs for the three $\phi = 17$ expansions. Here the $\eta_0 = 0.1667$ QSE cluster range is more limited than those in the other two expansions. The cause of this is the freezing out from the QSE. Figure 18 shows elemental abundances for the $\phi = 17$, $\eta_0 = 0.1667$ expansion during the evolution from $T_9 = 5.5$ to $T_9 = 4.5$. At $T_9 = 5.5$, the network abundances (*solid curve*) and the QSE abundances (*dotted curve*) agree well over the entire range in atomic number, and both differ greatly from the NSE distribution (*dashed curve*). The broad, flat QSE distribution reflects the broad, flat binding energy per nucleon curve in Figure 13, including the peak at ^{66}Ni and the sharp cutoffs below $Z = 20$ and above $Z = 38$. As the temperature falls, the QSE distribution moves to higher charge nuclei because the increasingly large excess of light particles relative to their NSE abundances allows the higher charge nuclei to compete more effectively for high abundance. The network distribution manages to keep pace with these changes until T_9 falls below 5.0. At this point, the abundances of protons and alpha particles falls to a sufficiently low level that they cannot shift upward the nuclei with $Z \lesssim 28$ as rapidly as QSE demands. The assembly of new heavy nuclei (see Fig. 11) compounds this effect by providing a current of new nuclei moving upward toward the Se-Kr peak. We will discuss this current in § 5. By $T_9 = 4.5$, elements below Ga no longer belong to the QSE cluster containing Se and Kr. The pattern of the network's abundance distribution is remarkable. The QSE and network abundances are in nearly perfect agreement for $Z \geq 32$, but the low-Z tail of the network distribution falls off much less steeply than that of the QSE. At this point in the expansion, a nearly divergenceless nuclear flow carries newly assembled nuclei from C up to the large QSE peak. Because the steady nuclear flow is given by a reaction cross section times an abundance, and since the cross sections decrease exponentially with increasing Z, abundances must increase exponentially with Z, as they do in Figure 18 for $T_9 = 4.5$. The jaggedness in the network abundance distribution results from the odd-even effect in nuclear binding.

The QSE and network elemental abundances also diverge above $Z \approx 43$ for $T_9 = 4.5$. This again results from the lack of sufficient protons to carry nuclei to higher charge. Despite the divergence of the network and QSE abundances for this expansion, it should be clear that the QSE distribution provides a excellent approximation to the most abundant species at $T_9 = 4.5$. Indeed, all nine expansions are well approximated by QSE at this temperature.

The solid curve in Figure 19 shows the elemental abundances for the $\phi = 17$, $\eta_0 = 0.1667$ calculation at $T_9 = 2$, near the final freezeout. Particularly interesting is the fact that the abundances of the elements below $Z = 35$ have grown since $T_9 = 4.5$, as seen by comparison with Figure 18. This results from continued assembly of heavy nuclei during this period. We tested this late assembly of heavy

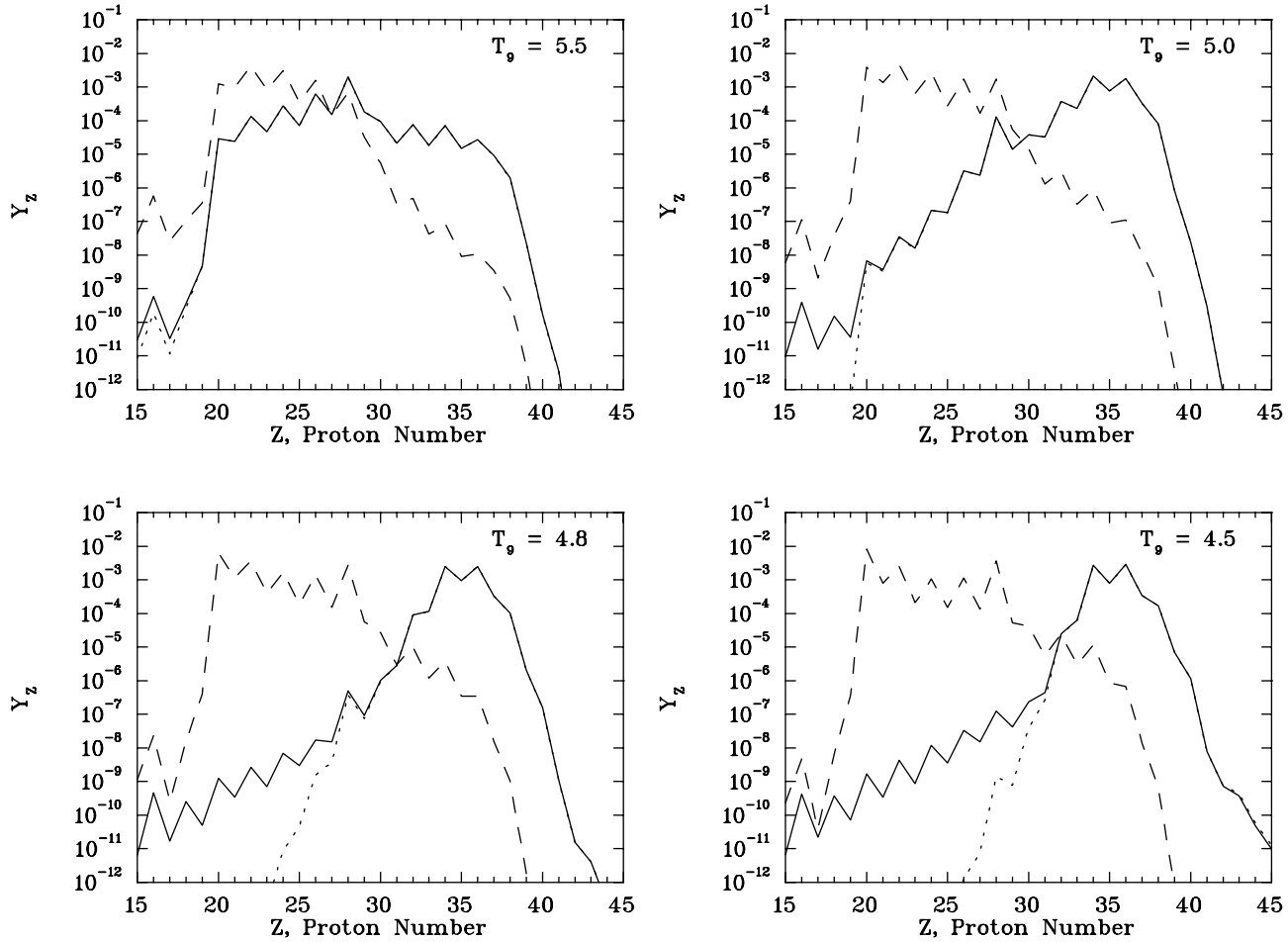

FIG. 18.—Elemental abundances during the $\phi = 17$, $\eta_0 = 0.1667$ expansion. The results are for the network (*solid curve*), NSE (*dashed curve*), and QSE (*dotted curve*). By $T_9 = 5.5$, the NSE abundances give a poor fit to the true (network) abundances. The QSE abundances continue to fit the true abundances well down to $T_9 = 4.5$, although lower Z elements begin dropping out of the QSE beginning at $T_9 = 5.5$. By $T_9 = 4.5$, the abundance of elements below Zn greatly exceed their QSE abundances. Ongoing formation of new heavy nuclei requires continued flow of these nuclei up to the QSE peak. As the temperature and light-particle densities fall, this flow becomes slower than QSE demands. The abundances of the lower Z elements thus diverge from QSE. The jaggedness in their abundance distribution results from the odd-even effect in the nuclear binding energies. Despite the divergence from QSE at lower proton number, the abundance peak in the network calculation at Se and Kr is still represented very well by QSE.

nuclei by running an identical calculation to the $\phi = 17$, $\eta_0 = 0.1667$ expansion except that this time we shut off the reactions assembling alpha particles into ^{12}C for $T_9 < 5$. The final elemental abundances are shown as the dashed curve in Figure 19. This distribution shows a much-depleted low-Z tail because of the lack of further assembly of heavy nuclei. We return to the question of the assembly of heavy nuclei in § 5.

4. APPROPRIATE TERMINOLOGY

Because the verbal images may cause confusion, it may be worthwhile to consider briefly the question of an appropriate astrophysical terminology. The term "alpha-rich freezeout" has been used to denote expansions of material that was once in NSE that cools with uncaptured alpha particles remaining abundant. We recommend adhering to that, in which case other explosive He-burning ejecta will not be so designated despite the similarity of hot free helium.

Less appropriate is the term "alpha process," coined by Woosley & Hoffman (1992) as shorthand for "the neutron-rich alpha-rich freezeout." In the first place, that term was one of those utilized by Burbidge et al. (1957) in their influential categories of nuclear processes. That process was not well delineated by them, and today we recognize its issues to be addressed by neon and silicon burning. Woosley & Hoffman (1992) preferred to appropriate that term to new usage because they perceived that excess neutrons change the nature of the alpha-rich freezeout in such ways that it is really a distinct process. They noticed that with increasing neutron richness, the alpha-rich freezeout builds to very much more massive nuclei, and they repeatedly use the image of (α, n)-reactions carrying this flow to larger atomic weights. We find grounds to question those terms.

Our calculations show that alpha reactions are of no more importance than any other reactions with free light particles. The nuclear network establishes a QSE for each neutron excess studied. The distinction is as follows. For low neutron excess, the QSE has rapidly falling abundances as ones moves attention toward massive n-rich nuclei. Those nuclei participate in the QSE, but their abundances are simply negligible. As the neutron excess is increased, however, the abundances of more massive n-rich nuclei in the QSE rise, giving the impression of a nuclear flow. Although it is obviously necessary for some nuclear flow to move nuclei from Zn, say, up to Sr, say, the actual nuclear

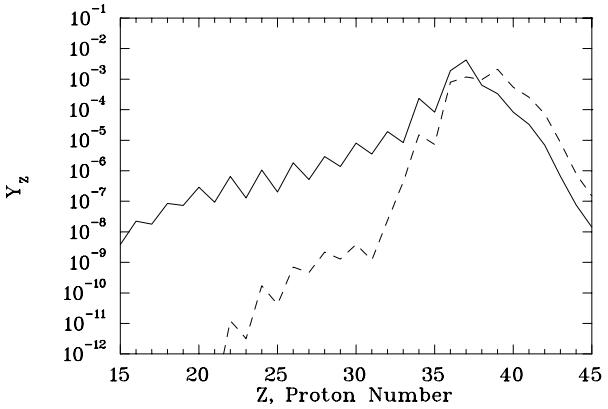

FIG. 19.—The elemental abundances for the $\phi = 17$, $\eta_0 = 0.1667$ expansion after reaction freezeout for a normal network calculation (*solid curve*) and for a network calculation in which the reactions assembling new heavy nuclei from alpha particles are disabled below $T_9 = 5.0$. Assembly of new heavy nuclei for $T_9 < 5$ has had important effects on the final abundance distribution for this expansion. Most importantly, the abundances of elements below Se are much less in the expansion that did not include heavy-nucleus assembly throughout. Because Y_h is fixed in this expansion for $T_9 < 5$, the abundance distribution, following QSE, shifts to higher atomic number, and the lack of further assembly of heavy nuclei prevents compensation of the depletion of the lower Z elements due to this shift. Comparison of the solid curve in this figure with that in the $T_9 = 4.5$ of Fig. 18 shows that there is significant assembly of new heavy nuclei for $T_9 < 4.5$.

rates would achieve this very quickly, much more quickly than it actually happens. Our Figure 10 of the reference calculation shows that the Sr peak grows as the QSE temperature falls from 5.85 to 4.03. The time required for this is almost 0.1 s, whereas the lifetime of a Ge isotope at $T_9 = 5$ against an (α, n)-reaction is about 10 μs, very much shorter. For this reason, the elemental abundance distribution at $T_9 = 5.85$ would transform to that at $T_9 = 4.03$ thousands of times more rapidly than it actually does were it simply a matter of (α, n)-reactions moving the material upward. What actually happens is that the QSE island, which is very large, shifts its shape as the temperature falls. When excess neutrons exist, as in the case of our reference calculation, the property of that QSE is that the heavy neutron-rich nuclei are much more abundant than they are at low neutron excess. But in either case they are in QSE; it is only the QSE abundances that so differ. This situation is little different in principle from that of the old NSE studies, where many showed that the abundance of ^{62}Ni, say, rises steeply as the neutron excess is increased above zero. This has nothing to do with nuclear flow, however, but simply the shape of the NSE.

Figure 8 may be seen in a new light. The fact that $R = 1$ down to $T_9 \approx 3.4$ shows that over that entire range the alpha particles are in QSE with p and n. Mechanistically, this means that the dominant cycles for fusing p and n into alpha particles run at the same rates as the inverse cycles breaking alpha particles down into p and n. For those cycles, it is not meaningful to say whether alpha- or nucleon-induced reactions are leading the way to QSE shape readjustments. They do so at almost equal rates. When the QSE finally does break down, the temperatures are low and the p- and n-reactions are even more effective than the alpha reactions in the final freezeout.

To illustrate these ideas, we performed a numerical experiment by rerunning the reference expansion with all alpha-induced reactions disabled for target elements having $Z > 28$. That is, only p- and n-induced reactions are allowed nonzero cross sections above the element nickel. The insensitivity of the results to this alteration is shown in Figure 20. Both calculations shown there utilize complete network expansions, but the solid abundance distribution was calculated with disabled alpha reactions, whereas the dashed distribution utilized the full set of reactions. Quite clearly the results are almost indistinguishable for the most abundant nuclei. The largest effect occurs at $Z = 32$ and 34, where alpha captures by the QSE $Z = 30$ peak have, during final freezeout, increased these small abundances owing to the huge abundance of their $Z = 30$ parents. Those are alpha freezeout reactions. But in the massive Sr peak, there is little difference of physical significance. The conclusion is that alpha-induced reactions play no special role in the transfer of nuclei from the Zn region to the Sr region. Indeed, one would expect that alpha freezeout reactions would be less important for the Sr peak because in the face of falling temperatures, the alpha particles will be captured by those abundant nuclei having smaller Coulomb barrier, namely the Ni and Zn peak. It therefore seems inadvisable to adopt the suggested terminology "alpha process" recommended by Woosley & Hoffman (1992), whose exploratory work opened up the study of the greatly increased abundances that do occur in high-entropy neutron-rich alpha-rich freezeouts. Their pioneering study was done before the QSE nature of their results was fully appreciated, so their image of how the abundance shifts occurs is inappropriate in some places.

We must address the Figure 6 presented by Woosley & Hoffman (1992). This figure shows, by arrow density, the strongest net flows (forward-backward) for reactions during

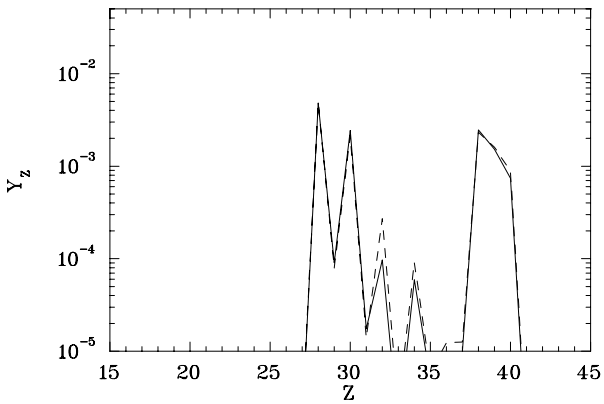

FIG. 20.—Comparison of the final abundances after freezing, obtained with the network solution, but with alpha-induced reactions given zero cross sections for elements above nickel (*solid curve*). The full network (*dashed curve*) is the same result of the reference calculation that was shown in Fig. 10. The role of alpha-induced reactions on final abundances is small. Only the $Z = 32$ and 34 subpeaks are enhanced owing to the freezeout capture of alpha particles. The Sr peak is hardly altered by alpha reactions by nuclei between the main peak (Ni) and this secondary peak. The alpha reactions are no more important than the nucleon-induced reactions in establishing that Sr peak because the QSE does not distinguish among alternate reaction paths. The lack of alpha-capture modifications of the Sr peak can also be understood; owing to its higher Coulomb repulsion than the Ni peak, the alpha captures occur primarily on the latter, with small p and n freezeout reactions altering the Sr peak. The term "alpha process" is therefore not appropriate for the alpha-rich freezeout. A consequence may be that the r-process seed nuclei (the Sr peak) can have their abundances within high-entropy neutron-rich alpha-rich freezeouts reliably estimated by a QSE distribution at freezeout $T_9 = 4$.

freezeout of a high-entropy neutron-rich freezeout of the type we discuss here. The three panels of that figure show the strongest flows at three separate temperatures, $T_9 = 4.0$, 3.23, and 2.49. The strength of the solid (α, n) arrows is pointed to by them as indicators that "movement up through the network (at $T_9 = 4.0$) is being carried by (α, n)-reactions." Because that statement and the arrows on those figure panels give a different impression than the conclusions that we are presenting, we call attention to the source of that discrepancy, which is more apparent than real.

We make two points. (1) Those figures do not show that a net flow is strong—only that it is strong when compared with other net flows. What the solid flow arrows designate are net reaction flows within a factor 0.1 of the strongest net flow in the diagram [which is $^{85}\mathrm{Se}(n, \gamma)^{86}\mathrm{Se}$-$^{86}\mathrm{Se}(\gamma, n)^{85}\mathrm{Se}$]. However, even those strong net flows are close to equilibrium with their reverse flows, so that all net flows are small in comparison with the forward flows. That is, the nuclear abundances at $T_9 = 4$ are nearly in QSE, as we have shown. The QSE is just beginning to break down at $T_9 = 4$, so that the modest importance of cross sections is just coming into its brief moment of relevance, but the main abundance features are already set by that QSE. It would have been more instructive to have designated net flows by multiples of the forward flow, in which case their low values would be in line with our demonstration that reaction cross sections are for the most part insignificant for this problem. (2) The strong arrows in their Figure 6*b* for $T_9 = 3.2$ look just as strong as at $T_9 = 4.0$, whereas they are very much smaller in value. Their magnitudes must be rescaled for comparison between the $T_9 = 4$ arrows and the $T_9 = 3.2$ arrows; however, our results show that the freezeout of the QSE below $T_9 = 4$ has little effect except for the final growth of some small abundances having abundant parents that were set by the QSE. At $T_9 = 3.2$, Woosley & Hoffman note that the net flow rate for the largest net flow, $^{87}\mathrm{Se}(n, \gamma)^{88}\mathrm{Se}$, has the value 0.0024 s^{-1}. By comparison, since the free neutron density is $n_n = 10^{27}$ cm^{-3}, the forward rate for ^{87}Se, with abundance $Y(^{87}\mathrm{Se}) = 10^{-4}$, for destruction by free neutrons is $(10^{-4})(10^{27}\ \mathrm{cm}^{-3})(10^{-26}\ \mathrm{cm}^2)(10^8\ \mathrm{cm\ s}^{-1}) = 10^5\ \mathrm{s}^{-1}$. This is 10^8 times faster than the net flow. Even this strongest flow is in tight QSE with neutrons. The reader must compare our work with the meaning of this informative figure by Woosley & Hoffman to understand that the discrepancy is only apparent.

We think that the term "alpha-rich freezeout" remains a good one and that it may best be taken to apply to circumstances in which material initially in NSE is unable, owing to the low density of high-entropy expansions and to a deficiency in the number Y_h of heavy nuclei, to capture the free alpha particles during the expansion. That term applies well whatever the neutron richness, for the sequence of events is the same. The NSE is restricted to a QSE by falling temperature. The QSE is alpha rich because Y_h is small. That QSE abundance distribution is insensitive to the values of nuclear reaction cross sections. Figure 20 shows that the same QSE distributions result whether alpha reactions are disabled or not. Even the free densities of p, n, and α at the time when the QSE is itself no longer capable of maintenance by the reactions are insensitive to nuclear cross sections. Only "the freezeout reactions," which we define as those that occur after the QSE has broken down, are dependent upon nuclear cross sections. To emphasize this once more, we would say that although the abundance of final Ge in Figure 20 depends upon the cross sections for alpha reactions with Zn, the abundance of Sr is almost independent of all alpha cross sections. We have asked the reader to proceed through these arguments because the situation may at first seem counterintuitive to some. It is only by digesting our results that we have become able to understand how these transitions occur and why some terminologies are less appropriate than others. Every terminology carries with it the burden of a physical association with its words, so that inappropriate terminology is not far removed from poor understanding to new workers.

5. ASSEMBLY OF HEAVY NUCLEI

The recognition of the quasi-equilibrium character of material expanding from high temperature would appear to make possible a simplification in the computation of nuclear yields. For example, we might imagine that we could determine the final abundances by simply freezing a QSE. This would require first specifying ρ, T_9, Y_e, and Y_h at $T_9 = 4$ to obtain the QSE distribution of nuclei and then using the nucleosynthesis network to follow the freezeout reactions as the material cooled below $T_9 = 4$. This would indeed be a great simplification because we would not need to run a network code above $T_9 = 4$. For some applications, the QSE abundances themselves may be sufficiently accurate, allowing a dispensing with nuclear reactions entirely. This procedure mimics earlier studies of freezeout of NSE by first determining NSE abundances at a "freezeout" temperature (say, $T_9 \approx 3.5$) and then following the subsequent freezeout reactions with a network code (e.g., Hartmann, Woosley, & El Eid 1985).

The difficulty with the QSE-based approach is that one must be able to specify Y_h, and that quantity depends on the nuclear history of the expansion. We could try the approach of specifying Y_e and Y_h at the QSE freezeout temperature. This would not give an accurate representation of the abundances emerging from particular expansion unless Y_e and Y_h were correctly chosen. We therefore set ourselves a larger challenge by attempting to find Y_h at the QSE freezeout temperature as accurately as possible but without using the reaction network. We pursue this to establish the point that final abundances can be estimated without a nuclear code; but we by no means advocate this as a practical research tool for nucleosynthesis, although similar techniques are being used in stellar evolution codes to limit the size of nuclear networks for study of advanced burning stages (e.g., Hix & Thielemann 1996).

The approach parallels older treatments of NSE and of the silicon-burning QSE. The idea for NSE evolution was to approximate network expansions by following the change in Y_e produced by an evolving NSE. The NSE abundances are computed at time t. The rate of change of Y_e, i.e., dY_e/dt, is then computed from the NSE abundances and the weak reaction rates. This allows an updating of Y_e over time step Δt: $\Delta Y_e = (dY_e/dt)\Delta t$. For silicon burning, the key parameter is Y_h, and the idea there was that, following the calculation of a QSE based on Y_h, that parameter could be altered by calculating the rate of ^{28}Si breakdown, whereupon the evolved QSE is updated.

We begin by noting that the nuclear flow from α-particles to heavy nuclei is through the three-body reaction sequences $\alpha + \alpha + \alpha \rightarrow {}^{12}\mathrm{C}$ and $\alpha + \alpha + n \rightarrow {}^{9}\mathrm{Be}$ followed by $^{9}\mathrm{Be}(\alpha, n)^{12}\mathrm{C}$. We assume that these are followed by a rapid run to larger atomic weight, so that the assembly of a

^{9}Be or ^{12}C nucleus is the assembly of a general heavy nucleus; therefore,

$$\frac{dY_h}{dt} = \frac{(N_A\rho)^2\langle\sigma v\rangle_{3\alpha} Y_\alpha^3}{3!} - \lambda_{3\alpha} Y_{^{12}C} + \frac{(N_A\rho)^2\langle\sigma v\rangle_{\alpha\alpha n} Y_\alpha^2 Y_n}{2!} - \lambda_{\alpha\alpha n} Y_{^9Be} . \quad (33)$$

In this equation, $\langle\sigma v\rangle_{3\alpha}$ is the triple-α velocity-averaged cross section, $\lambda_{3\alpha}$ is the rate for the reverse reaction $^{12}C \rightarrow \alpha + \alpha + \alpha$, $\langle\sigma v\rangle_{\alpha\alpha n}$ is the velocity-averaged cross section for the $\alpha + \alpha + n \rightarrow {}^9$Be reaction, and $\lambda_{\alpha\alpha n}$ is the rate for the reverse reaction $^9\text{Be} \rightarrow \alpha + \alpha + n$. From detailed balance (the requirement that reverse flows balance forward flows in NSE), we find

$$\frac{(N_A\rho)^2\langle\sigma v\rangle_{3\alpha}(Y_\alpha^{NSE})^3}{3!} = \lambda_{3\alpha} Y_{^{12}C}^{NSE} \quad (34)$$

and

$$\frac{(N_A\rho)^2\langle\sigma v\rangle_{\alpha\alpha n}(Y_\alpha^{NSE})^2 Y_n^{NSE}}{2!} = \lambda_{\alpha\alpha n} Y_{^9Be}^{NSE} . \quad (35)$$

With these equations, we find

$$\frac{dY_h}{dt} = \frac{(N_A\rho)^2\langle\sigma v\rangle_{3\alpha}(Y_\alpha^{NSE})^3}{3!}\left[\left(\frac{Y_\alpha}{Y_\alpha^{NSE}}\right)^3 - \left(\frac{Y_{^{12}C}}{Y_{^{12}C}^{NSE}}\right)\right] \quad (36)$$

$$+ \frac{(N_A\rho)^2\langle\sigma v\rangle_{\alpha\alpha n}(Y_\alpha^{NSE})^2 Y_n^{NSE}}{2!} \times \left[\left(\frac{Y_\alpha}{Y_\alpha^{NSE}}\right)^2\left(\frac{Y_n}{Y_n^{NSE}}\right) - \left(\frac{Y_{^9Be}}{Y_{^9Be}^{NSE}}\right)\right] . \quad (37)$$

Integration still requires a nuclear network to solve equation (37) because we need to know $Y_{^9Be}$ and $Y_{^{12}C}$. In keeping with the challenge we set ourselves, however, we seek to avoid using the network. We can attempt this by assuming that ^{9}Be and ^{12}C are in the QSE cluster with the other heavy nuclei. In this case, $Y_{^{12}C}/Y_{^{12}C}^{NSE} = e^{\mu_h/kT}R_\alpha^3$ and $Y_{^9Be}/Y_{^9Be}^{NSE} = e^{\mu_h/kT}R_\alpha^2 R_n$. Equation (37) now becomes

$$\frac{dY_h}{dt} = \frac{(N_A\rho)^2\langle\sigma v\rangle_{3\alpha}(Y_\alpha^{QSE})^3}{3!}(1 - e^{\mu_h/kT}) + \frac{(N_A\rho)^2\langle\sigma v\rangle_{\alpha\alpha n}(Y_\alpha^{QSE})^2 Y_n^{QSE}}{2!}(1 - e^{\mu_h/kT}) . \quad (38)$$

It is now possible to integrate Y_h without using the reaction network.

Before integrating equation (38), we note certain of its features. First, if the system is in complete NSE, $\mu_h = 0$. In this case, $dY_h/dt = 0$, as expected. What equation (38) shows is that, even at high temperature and density, where forward and reverse reaction rates are huge, an evolving system can never be in precise NSE. In order to allow a change in Y_h, μ_h must be at least slightly different from zero. If $\mu_h < 0$, $dY_h/dt > 0$, and heavy nuclei are produced. If $\mu_h > 0$, $dY_h/dt < 0$, and heavy nuclei are destroyed.

An analogy may help at this point. In the interior of stars, the radiation field is extremely close to isotropic. It is not precisely isotropic, however, because in that case there is no net energy flow. It is the small negative temperature gradient that allows a net energy flow outward from the star's center. By analogy, it is the tiny deviation of μ_h from zero that allows a change in Y_h, even at high temperature.

TABLE 1

LIMITED NUCLEAR NETWORK

Element	A_{min}	A_{max}	Element	A_{min}	A_{max}
n	1	1	K.....	35	48
H	1	3	Ca	36	49
He	3	4	Sc	40	49
C.....	12	12	Ti	42	42
O	16	16	V.....	43	53
Ne	20	20	Cr.....	44	54
Mg.....	24	24	Mn.....	46	59
Si	28	28	Fe.....	47	60
P	27	34	Co	50	63
S	28	37	Ni.....	51	65
Cl	31	40	Cu	57	70
Ar.....	32	43	Zn	59	71

We attempted an integration of equation (38) with our QSE solver. Our procedure was as follows. We began at $t = 0$ with $T_9 = 7$ and the nuclei in NSE. The calculation for this analysis used $\phi = 6.8$, $\eta_0 = 0.0$, and $\tau = 0.2$ s. At time t, we computed QSE abundances and $\mu_h(t)$ from $T_9(t)$, $\rho(t)$, $Y_e = 0.5$ (fixed in this calculation), and $Y_h(t)$. We then used $Y_\alpha^{QSE}(t)$, $\mu_h(t)$, and $T_9(t)$ to compute dY_h/dt from equation (38) and to integrate Y_h to time $t + \Delta t$. Our actual integration scheme was fourth-order Runge-Kutta. We integrated Y_h down to $T_9 = 2$. We did not calculate weak decays because our interest lies in testing the quality of the nuclear network approximation.

To this end, we used for simplicity the more limited network shown in Table 1 for the integration of equation (38). The smaller network speeds up our calculations. Our choice of $\eta_0 = 0.0$ ($Y_e = 0.5$) is appropriate for this smaller network. The network is monoisotopic for elements between carbon and magnesium. The reason for this choice will become clear below. The lack of ^{9}Be in the network means only the triple-α reaction assembled light particles into heavy nuclei.

Figure 21 shows the result of this calculation for Y_h. The solid curve is the integration for Y_h using QSE abundances

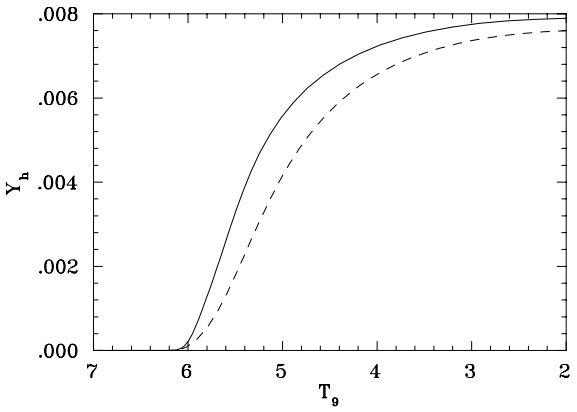

FIG. 21.—Y_h in the $\eta_0 = 0.0$, $\phi = 6.8$ expansion for the network shown in Table 1 as determined from integration of eq. (38) (*solid curve*) and from the full nuclear reaction network (*dashed curve*). Integration of eq. (38) fails to match the full network calculation because a fundamental assumption of eq. (38), viz., that ^{12}C is always in QSE, is incorrect (see Fig. 22).

for all nuclei. Shown for comparison as the dashed curve is the corresponding network calculation of Y_h using the network in Table 1. In this network calculation, we turned off weak reactions so Y_e would be constant. This allowed for more consistent comparison with the integration of equation (38), although the difference between the network calculation with and without weak reactions was small. The two curves differ significantly throughout the expansion. The assumption that all nuclei are in QSE must be incorrect. This failure of the simplest integration scheme brings out an important aspect of QSE nucleosynthesis.

The reason for the failure is apparent in Figure 22*a*. This figure shows $Y(^{12}\mathrm{C})$ in the network (*solid curve*), in NSE (*long-dashed curve*), and in QSE (*dotted curve*) for the reaction network calculation. Significantly, the network abundance of ^{12}C is considerably greater than the QSE value below $T_9 = 6.2$. A fundamental assumption of equation (38) thereby breaks down. Because ^{12}C is significantly more abundant in the network calculation than in QSE for $T_9 < 6.2$, there are much greater disintegration flows from $^{12}\mathrm{C} \rightarrow \alpha + \alpha + \alpha$. This hinders the assembly of heavy nuclei and prevents Y_h in the network calculations (Fig. 21, *dashed curve*) from reaching as large a value as in the simple integration (Fig. 21, *solid curve*) of equation (38). For comparison, Figure 22*b* shows $Y(^{28}\mathrm{Si})$ in the same formats. Unlike the ^{12}C, the ^{28}Si remains in QSE down to $T_9 \approx 5$. Although QSE tracks $X(^{28}\mathrm{Si})$ faithfully, below $T_9 = 4.8$ its actual but small abundance increasing exceeds the vanishing QSE abundance. Note also the smallness of the mass fractions of both nuclei and that both increase during the freezeout owing to the continuing occurrence of the triple-α reaction and upward flow to ^{28}Si.

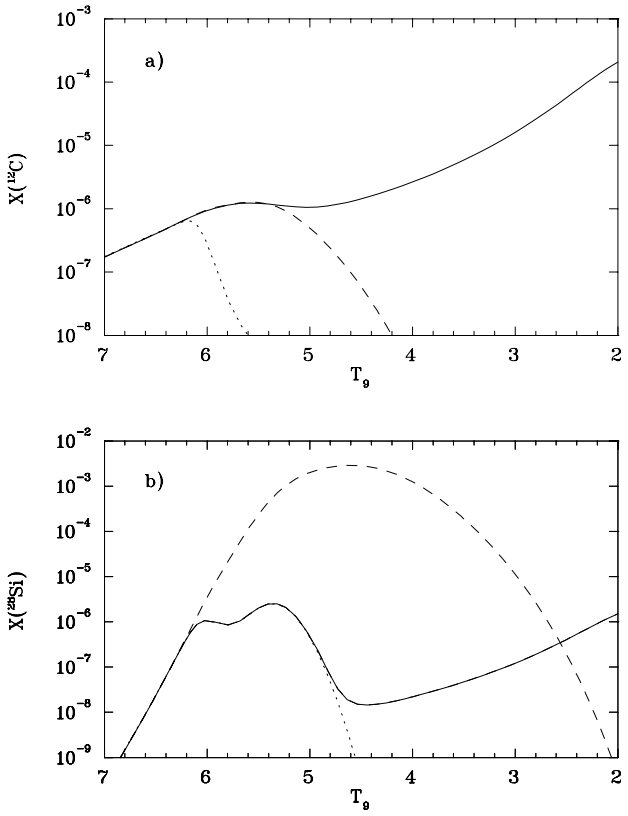

FIG. 22.—Mass fractions of (*a*) ^{12}C and (*b*) ^{28}Si during the $\eta_0 = 0.0$, $\phi = 6.8$ expansion using the nuclear reaction network. The different curves give the network (*solid curve*), NSE (*dashed curve*), and QSE (*dotted curve*) abundances during the expansion. ^{12}C falls out of QSE early ($T_9 > 6$). This causes the failure of the integration of eq. (38) to match the network's Y_h. By contrast, QSE matches the network's ^{28}Si mass fraction well down to $T_9 \approx 4.8$. This leads us to try a new integration of dY_h/dt by assuming ^{28}Si is always in QSE and a divergenceless flow moves nuclei from ^{12}C to ^{28}Si. The result of these assumptions is eq. (44), and the integration is shown in Fig. 23. A very curious feature of panel (*a*) is the fact that NSE provides a better fit to the network's mass fraction of ^{12}C than does QSE for $T_9 < 6.4$. For $T_9 < 6.4$, the ^{12}C abundance is set not by the QSE, but rather by the divergenceless flow. This flow is governed by the competition between local captures and disintegrations, which aligns the ^{12}C more with NSE than QSE.

Despite the fact that ^{12}C falls out of the QSE at relatively high temperature, a nearly divergenceless net flow runs upward from that nucleus to the QSE cluster. Good analogy exists with silicon burning, where nuclei above ^{24}Mg are in QSE but ^{20}Ne and below are not (Bodansky et al. 1968). Because silicon burning has *more* nuclei than NSE, the evolution in that case *reduces* the number Y_h within the QSE cluster. It does so by a nearly divergenceless disintegration flow *down* from ^{28}Si to ^{4}He. We can, in the present case, proceed analogously to the calculation in Bodansky et al. (1968) to compute $J(^A Z)$, the upward flow at each species $^A Z$. For the simplified network in Table 1, we find

$$J(^4\mathrm{He}) = \frac{(N_\mathrm{A}\rho)^2\langle\sigma v\rangle_{3\alpha}(Y_\alpha)^3}{3!} - \lambda_{3\alpha}\, Y(^{12}\mathrm{C})\,, \quad (39)$$

$$J(^{12}\mathrm{C}) = N_\mathrm{A}\langle\sigma v\rangle_{12}\,\rho Y_\alpha\, Y(^{12}\mathrm{C}) - \lambda_{\gamma 16}\, Y(^{16}\mathrm{O})\,, \quad (40)$$

$$J(^{16}\mathrm{O}) = N_\mathrm{A}\langle\sigma v\rangle_{16}\,\rho Y_\alpha\, Y(^{16}\mathrm{O}) - \lambda_{\gamma 20}\, Y(^{20}\mathrm{Ne})\,, \quad (41)$$

$$J(^{20}\mathrm{Ne}) = N_\mathrm{A}\langle\sigma v\rangle_{20}\,\rho Y_\alpha\, Y(^{20}\mathrm{Ne}) - \lambda_{\gamma 24}\, Y(^{24}\mathrm{Mg})\,, \quad (42)$$

and

$$J(^{24}\mathrm{Mg}) = N_\mathrm{A}\langle\sigma v\rangle_{24}\,\rho Y_\alpha\, Y(^{24}\mathrm{Mg}) - \lambda_{\gamma 28}\, Y(^{28}\mathrm{Si})\,. \quad (43)$$

Because the (α, γ)-reactions and their inverses are rapid compared to the rates at which the abundances of C, O, Ne, and Mg change, the flow from ^{4}He to the QSE cluster must evidently be divergenceless, and all of the $J(^A Z)$'s take on the same value J. Although C, O, Ne, and Mg are not now constrained to be within the QSE cluster, their abundances nonetheless take on stationary values determined by the divergencelessness of J. With the assumption that ^{28}Si participates in the QSE cluster, we find

$$J = \frac{r_{3\alpha}\, Y_\alpha^3(1 - e^{\mu_h/kT})}{1 + (\gamma/\alpha)_{12}(1 + (\gamma/\alpha)_{16}\{1 + (\gamma/\alpha)_{20}[1 + (\gamma/\alpha)_{24}]\})}\,, \quad (44)$$

where

$$r_{3\alpha} = \frac{(N_\mathrm{A}\rho)^2\langle\sigma v\rangle_{3\alpha}}{3!}\,, \quad (45)$$

and $(\gamma/\alpha)_A$ is the ratio of the disintegration rate at A to the capture rate at A. For example,

$$\left(\frac{\gamma}{\alpha}\right)_{16} = \frac{\lambda_{\gamma 16}}{N_\mathrm{A}\langle\sigma v\rangle_{16}\,\rho Y_\alpha}\,. \quad (46)$$

Because J is the net flow up from ^{4}He, it is in fact dY_h/dt. We now use this equation to integrate Y_h.

Before considering the results, note key features of equation (44). First, the numerator is the same as in equation (38), which is restricted by the network in Table 1 to utilize only the triple-α reaction. Thus, the assembly of

heavy nuclei derives from this reaction, but it is driven by the deviation from NSE (the $1 - e^{\mu_h/kT}$ term). Equation (38) and (44) differ only by the presence of the denominator in the latter equation. This term governs how a newly assembled ^{12}C nucleus actually works its way up to ^{28}Si. If $(\gamma/\alpha)_{12}$ is large, for example, the ^{12}C is more likely to disintegrate back into alpha particles than to capture up to ^{16}O. This decreases the net flow up to the QSE cluster. Competition between disintegration and capture at oxygen, neon, and magnesium similarly influence the flow upward through them.

Figure 23 shows Y_h from equation (44). For comparison, Y_h as computed with the nuclear reaction network code is shown as the dashed curve. The agreement is to within 2%. This is a considerable improvement over the previous integration (Fig. 21) based on assuming ^{12}C to be in the QSE cluster. The remaining discrepancy in Figure 23 is apparently due to the small deficit (on the order of 2%) of $Y(^{28}Si)$ in QSE from its true value in the network expansion for $T_9 \approx 6$. This leads to a slightly lower disintegration flow down from ^{28}Si for QSE abundances, which hinders the assembly of heavy nuclei less than in the network. Nonetheless, the good agreement in Figure 23 confirms the correctness of the approach taken and that the final abundances can, in principle, be estimated without a reaction network.

It is useful to consider separately the behavior of each part of equation (44) during the expansion. Figure 24 shows the factor $1 - \exp(\mu_h/kT)$ during the expansion. For $T_9 > 6.4$, this factor is extremely small, which shows the system is close to NSE. The system has almost exactly its desired number of heavy nuclei, so the assembly rate is small. This driving factor grows rapidly for $T_9 < 6.4$, however, which impels the system to create new heavy nuclei. Once this factor is close to unity, the system is demanding creation of new heavy nuclei as rapidly as possible. The assembly is blocked, however, by the disintegrations of the carbon, oxygen, neon, and magnesium nuclei. This term is the denominator in equation (44). Its value during the expansion is shown in Figure 25. Its value is substantial, especially for $T_9 > 5$. Initially, at $T_9 = 7$, the photodisintegrations

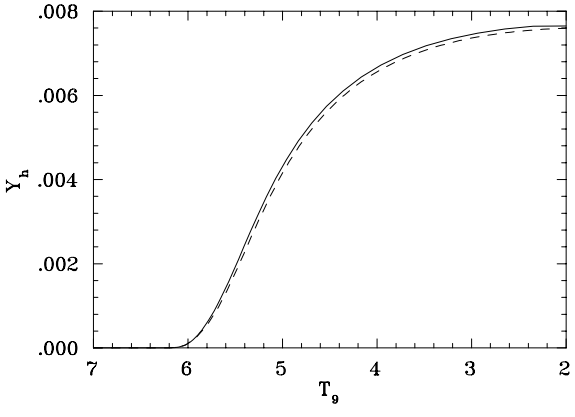

FIG. 23.—Y_h in the $\eta_0 = 0.0$, $\phi = 6.8$ expansion for the network shown in Table 1 as determined from integration of eq. (44) (*solid curve*) and from the full nuclear reaction network (*dashed curve*). This integration is more accurate than that shown in Fig. 21 and shows that the assumptions that ^{28}Si is always in QSE and that a divergenceless flow carries nuclei from ^{12}C to ^{28}Si are more correct than the assumption that ^{12}C is always in QSE. The success of this calculation (to within ~2%) suggests abundance yields from many expansions can be estimated to reasonable accuracy without a nuclear reaction network.

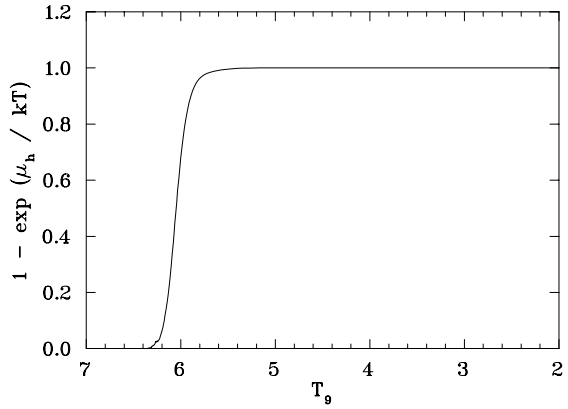

FIG. 24.—Evolution of the driving factor $1 - \exp(\mu_h/kT)$ during the integration of eq. (44). This factor represents the deviation from NSE. At high temperatures, it is close to zero, which indicates that the system has the number of heavy nuclei NSE demands. Over a short drop in temperature (from $T_9 \approx 6.4$ to $T_9 \approx 5.6$), this factor rises quickly to a value near unity. This indicates a serious underabundance of heavy nuclei in the system relative to NSE and strongly compels the system to assemble new heavy nuclei.

reduce the upward flow by a factor exceeding 10^3. For $T_9 < 5$, however, the excess of alpha particles in this alpha-rich freezeout and the much-reduced disintegration rates allow newly created ^{12}C nuclei to move up unimpeded to silicon. Figure 26 shows J during the expansion (*solid curve*). For comparison, the magnitude of $r_{3\alpha} Y_\alpha^3$ is shown as the dashed curve. Early in the expansion, $r_{3\alpha} Y_\alpha^3$ is large, but the net rate is small because the deviation from NSE $1 - e^{\mu_h/kT}$ is small (Fig. 24), and newly created ^{12}C nuclei are blocked from capturing up to silicon (Fig. 25). As the temperature drops, $r_{3\alpha} Y_\alpha^3$ decreases, but the growth in the deviation from NSE and the drop in the blockage from disintegrations (the denominator in eq. [44]) cause J to rise. Once the impedance from disintegration becomes negligible, $J \rightarrow r_{3\alpha} Y_\alpha^3$.

Our success in integrating dY_h/dt relied on our ability to identify a nucleus (^{28}Si) participating in the QSE cluster to a sufficiently low temperature and on the possibility of determining the exact flows from ^{12}C to that nucleus. This was

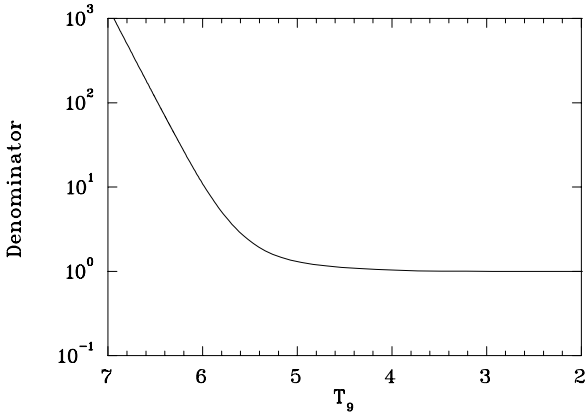

FIG. 25.—Evolution of the impedance factor in the denominator of eq. (44) during integration of dY_h/dt. This factor gives the blockage of flow from ^{12}C to ^{28}Si due to disintegrations of carbon, oxygen, neon, and magnesium. This factor is large in the early stages of the expansion. At this point the flow to ^{28}Si is slow. By $T_9 \approx 5$, the temperature is small enough and the alpha density large enough that captures on C, O, Ne, and Mg completely dominate disintegrations and the flow to ^{28}Si is unimpeded.

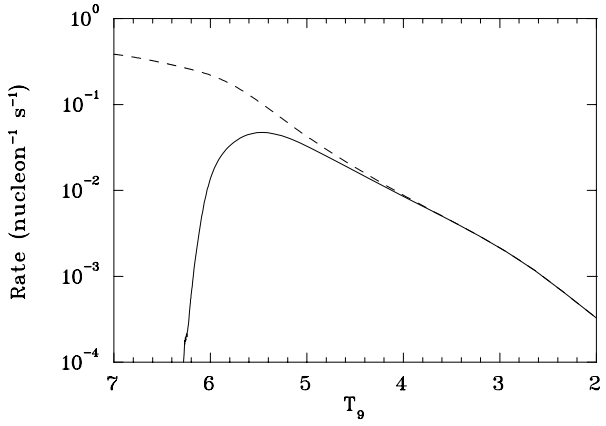

FIG. 26.—Net upward current J (*solid curve*) and the triple-α flow $r_{3\alpha}\, Y_\alpha^3$ (*dashed curve*) during integration of eq. (44). At early stages in the expansion, J is much less than the triple-α flow because the driving factor is small (Fig. 24) and the disintegration impedance is large (Fig. 25). As the temperature drops, both of these factors approach unity, and $J \rightarrow r_{3\alpha}\, Y_\alpha^3$. Thus, late in the expansion, the rate of growth of Y_h is simply the triple-α flow. Note that this drops with falling temperature so that assembly of new heavy nuclei eventually freezes out like the other nuclear reactions.

easy for the simplified network in Table 1, which was constructed to make the integration easy. For the more complicated networks used in the calculations presented in § 3, this is a more difficult matter. Those networks have many more isotopes for each element above and including carbon; thus, the identification of the flows up to the QSE cluster is much less straightforward. Nevertheless, a similar integration of dY_h/dt for those neutron-rich networks is also possible, at least in principle. We are satisfied that we answered the challenge we posed for ourselves at the beginning of this section. It would be possible to estimate the final abundances without integration of a full reaction network.

Of course, in general it is best to integrate the reaction network. In this case, there is no need to identify specific reaction pathways, and we can follow the nonequilibrium freezeout phenomena accurately. On the other hand, our attempts to integrate dY_h/dt have led to new insights into the assembly of heavy nuclei from light particles.

In closing this section, it is worthwhile noting that the expression for J, the net disintegration flow from ^{28}Si during silicon burning, as presented in Bodansky et al. (1968), can be recast into the language of the present work as

$$J = \frac{\lambda_{\gamma 24}\, Y(^{24}\mathrm{Mg})(1 - e^{\mu_h/kT})}{1 + (\alpha/\gamma)_{20}\{1 + (\alpha/\gamma)_{16}[1 + (\alpha/\gamma)_{12}]\}} \,. \qquad (47)$$

This provides a clear picture of silicon burning. The shocked Si shell in a supernova initially is far from NSE. This system has ^{28}Si, but ^{56}Ni is favored statistically; thus, the system has twice its desired Y_h. QSE quickly establishes itself among the nuclei heavier than and including ^{24}Mg, but because of the excess nuclei, μ_h is positive. This makes J negative, which indicates a strong impetus to disintegrate some of the ^{28}Si to decrease Y_h. Alpha captures on magnesium, neon, oxygen, and carbon oppose this disintegration and cause the magnitude of J to be smaller than simply the disintegration rate of ^{28}Si. As the burning continues, $Y_h \rightarrow Y_{h\mathrm{NSE}}$ and $\mu_h \rightarrow 0$. This causes $J \rightarrow 0$ as the system relaxes to NSE. It is rewarding, but in retrospect inevitable, that further insights into QSE nucleosynthesis can shed new light on the old problem of silicon burning. One might even say that the QSE concept reduces complexity to intellectually comprehensible levels for these problems.

6. CONCLUSION

We believe that the QSE theory set forth in this paper opens new windows on nucleosynthesis. The crucial idea of the extensive QSE phase during expansion of matter from high temperature permits a much better estimation of the resulting abundance yields than the notion of a "freezeout from NSE." Furthermore, QSE theory explains the nuclear dynamics of high-entropy expansions systems better than an appeal to net alpha capture flows. In essence, it reduces complexity to a comprehensible level.

At a perhaps deeper level, QSE theory helps explicate the emergence of order in high-temperature nucleosynthetic systems. A QSE, because of the added constraint imposed on it, is already a vastly more ordered state than NSE. The number of abundance states within the QSE constraint is very much less than the number available to the unconstrained NSE. What is more, as shown in § 2.4, the QSE discussed in this paper is but one of many possible statistical equilibria in a hierarchy of statistical equilibria in nucleosynthesis (see also the contribution by Meyer in Wallerstein et al. 1997). A system ascends the hierarchy by removing constraints. For example, if a system is heated, the reactions assembling heavy nuclei become sufficiently rapid that the number of heavy nuclei is no longer constrained to be fixed. This causes the QSE to go to NSE, and the system becomes more disordered. On the other hand, if some reaction between species within a QSE cluster becomes slow, the QSE cluster may break into two separate clusters, each with its own fixed number of nuclei. At this moment an additional constraint appears, and the system becomes more ordered. This process continues as the two clusters break up into three clusters, four clusters, five clusters, and so on. Each of these breakups adds a constraint and imposes more order on the system. In this way the system evolves to its final, frozen-out, fully ordered state. In fact, the expansions we have described in this paper evolve through such a series of increasingly constrained equilibria—we have simply chosen in this paper to emphasize the most basic of these because of its importance. It is evident that the concept of "freezeout" should be replaced in large measure by the notion of "descent of the hierarchy of statistical equilibria." This latter picture better connects nucleosynthesis with the underlying statistical physics. Finally, at the very end of the expansion, a few individual light particles are captured at rates that do depend upon individual cross sections. This final freezeout is a modest adjustment, which is important for rare species, but only marginally so for the major species produced.

The authors gratefully acknowledge discussions with J. R. Ray, W. R. Hix, and F.-K. Thielemann and help from L.-S. The. This work was supported by NASA grants NAGW-3480 and NAGW-2305.

Note added in manuscript.—In the original manuscript, we derived the QSE theory for an isolated system. For such a system, the total energy is constant, and we maximized the entropy subject to the appropriate constraints. In our network calculations, however, we in fact took the system to be in thermal contact with a heat bath with a specified

temperature. After the manuscript was accepted, we changed our derivation of the QSE theory to that in the present version, namely, one for a system in thermal contact with a heat bath, in order to be more consistent with our network calculations. The key results, however, and especially equation (27), are the same in both pictures. For a sketch of the derivation of the QSE theory for the thermally isolated system, please see the contribution of Meyer to Wallerstein et al. (1997).

REFERENCES

Arnett, W. D. 1996, Supernovae and Nucleosynthesis (Princeton: Princeton Univ. Press)
Bodansky, D., Clayton, D. D., & Fowler, W. A. 1968, ApJS, 16, 299
Burbidge, E. M., Burbidge, G. R., Fowler, W. A., & Hoyle, F. 1957, Rev. Mod. Phys., 29, 547
Caughlan, G. R., & Fowler, W. A. 1988, At. Data Nucl. Data Tables, 40, 283
Clayton, D. D. 1983, Principles of Stellar Evolution and Nucleosynthesis (Chicago: Univ. of Chicago Press), chapt. 7
———. 1998, Meteoritics Planet. Sci., submitted
Hartmann, D. H., Woosley, S. E., & El Eid, M. F. 1985, ApJ, 297, 837
Hix, W. R., & Thielemann, F.-K. 1996, ApJ, 460, 869
Hoyle, F. 1946, MNRAS, 106, 343
Kauffman, S. 1995, At Home in the Universe (New York: Oxford Univ. Press)
Meyer, B. S., Krishnan, T. D., & Clayton, D. D. 1996, ApJ, 462, 825
Thielemann, F.-K., Hashimoto, M., & Nomoto, K. 1990, ApJ, 349, 222
Wallerstein, G., et al. 1997, Rev. Mod. Phys., 69, 995
Woosley, S. E., Arnett, W. D., & Clayton, D. D. 1973, ApJS, 26, 231
Woosley, S. E., & Hoffman, R. D. 1992, ApJ, 395, 202